ORIGINAL ARTICLE

JBMR

Hexa-D-Arginine Treatment Increases 7B2•PC2 Activity in *hyp*-Mouse Osteoblasts and Rescues the *HYP* Phenotype

Baozhi Yuan,[1] Jian Q Feng,[2] Stephen Bowman,[1] Ying Liu,[2] Robert D Blank,[1] Iris Lindberg,[3] and Marc K Drezner[1]

[1]Department of Medicine, University of Wisconsin-Madison and Geriatric Research and Education Center, William S. Middleton Memorial Veterans Hospital, Madison, WI, USA

[2]Department of Biomedical Sciences, Baylor College of Dentistry, Texas A&M Health Science Center, Dallas, TX, USA

[3]Department of Anatomy and Neurobiology, University of Maryland Baltimore, Baltimore, MD, USA

ABSTRACT

Inactivating mutations of the "phosphate regulating gene with homologies to endopeptidases on the X chromosome" (*PHEX/Phex*) underlie disease in patients with X-linked hypophosphatemia (XLH) and the *hyp*-mouse, a murine homologue of the human disorder. Although increased serum fibroblast growth factor 23 (FGF-23) underlies the *HYP* phenotype, the mechanism(s) by which PHEX mutations inhibit FGF-23 degradation and/or enhance production remains unknown. Here we show that treatment of wild-type mice with the proprotein convertase (PC) inhibitor, decanoyl-Arg-Val-Lys-Arg-chloromethyl ketone (Dec), increases serum FGF-23 and produces the *HYP* phenotype. Because PC2 is uniquely colocalized with PHEX in osteoblasts/bone, we examined if PC2 regulates PHEX-dependent FGF-23 cleavage and production. Transfection of murine osteoblasts with PC2 and its chaperone protein 7B2 cleaved FGF-23, whereas *Signe1* (7B2) RNA interference (RNAi) transfection, which limited 7B2 protein production, decreased FGF-23 degradation and increased *Fgf-23* mRNA and protein. The mechanism by which decreased 7B2•PC2 activity influences *Fgf-23* mRNA was linked to reduced conversion of the precursor to bone morphogenetic protein 1 (proBMP1) to active BMP1, which resulted in limited cleavage of dentin matrix acidic phosphoprotein 1 (DMP1), and consequent increased *Fgf-23* mRNA. The significance of decreased 7B2•PC2 activity in XLH was confirmed by studies of *hyp*-mouse bone, which revealed significantly decreased *Sgne1* (7B2) mRNA and 7B2 protein, and limited cleavage of proPC2 to active PC2. The expected downstream effects of these changes included decreased FGF-23 cleavage and increased FGF-23 synthesis, secondary to decreased BMP1-mediated degradation of DMP1. Subsequent Hexa-D-Arginine treatment of *hyp*-mice enhanced bone 7B2•PC2 activity, normalized FGF-23 degradation and production, and rescued the *HYP* phenotype. These data suggest that decreased PHEX-dependent 7B2•PC2 activity is central to the pathogenesis of XLH. © 2013 American Society for Bone and Mineral Research.

KEY WORDS: X-LINKED HYPOPHOSPHATEMIA; *hyp*-Mouse; 7B2; SPC2; HEXA-d-ARGININE; fgf-23; BONE; RICKETS; OSTEOMALACIA

Introduction

X-linked hypophosphatemia (XLH) is the archetypal vitamin D–resistant disease in man, characterized by renal phosphate (Pi) wasting with resultant hypophosphatemia, abnormal vitamin D metabolism, defective bone and cartilage mineralization, dentine defects, and stunted growth.[1] Using positional cloning techniques, a gene involved in the pathogenesis of XLH was identified[2] and designated as "phosphate regulating gene with homologies to endopeptidases on the X chromosome" (*PHEX/Phex*). Subsequently, more than 280 loss-of-function mutations in *PHEX* have been reported in patients with XLH.[3–6] The murine homologue of the human disease, the *hyp*-mouse, has a phenotype identical to that evident in patients with XLH, and is due to a large deletion in the 3′ region of the *Phex* gene.[7] These findings suggest that a mutation in the *PHEX/Phex* gene is responsible for the phenotypic changes both in patients with XLH and the *hyp*-mouse.

Recent studies have begun to clarify the mechanism(s) that leads to the biochemical and skeletal abnormalities evident in

Received in original form April 3, 2012; revised form July 31, 2012; accepted August 2, 2012; accepted manuscript online August 9, 2012.

Address correspondence to: Marc K Drezner, MD, 4246 Health Sciences Learning Center, University of Wisconsin School of Medicine and Public Health, 750 Highland Avenue, Madison, WI, 53705, USA. E-mail: mkd@medicine.wisc.edu

Additional Supporting Information may be found in the online version of this article.

Journal of Bone and Mineral Research, Vol. 28, No. 1, January 2013, pp 56–72
DOI: 10.1002/jbmr.1738

patients with XLH and in the *hyp*-mouse. Several reports have established that fibroblast growth factor 23 (FGF-23) plays a central role in phosphate homeostasis. Autosomal dominant hypophosphatemic rickets (ADHR) arises from mutations in the gene encoding FGF-23,[8] which disrupts the consensus sequence (RXXR) for prohormone convertase (PC)-mediated proteolytic cleavage of FGF-23, resulting in increased circulating levels of the intact biologically active form of the protein.[9,10] In contrast, a distinct set of *FGF-23* mutations cause hyperphosphatemic tumoral calcinosis (HPTC) by decreasing either the amount or activity of intact FGF-23.[11–16] Finally, transgenic mice overexpressing FGF-23 (under the control of the α1(I) collagen promoter) exhibit growth retardation, osteomalacia, and disturbed phosphate homeostasis, consistent with abnormalities in patients with XLH.[17,18]

A central role for FGF-23 in the pathophysiology of XLH has been confirmed by the presence of increased circulating levels of FGF-23 in affected patients[19,20] and in *hyp*-mice,[21] and by reports establishing that the effects of the single phosphatonin, FGF-23, underlie all elements of the characteristic abnormalities comprising the renal and bone phenotype in XLH.[21,22] Moreover, studies in the *hyp*-mouse have shown that the increased circulating levels of FGF-23 result both from inhibited degradation of full-length FGF-23 to biologically inactive products, and enhanced production of FGF-23, consistent with observations of increased *Fgf-23* mRNA.[22,23]

Nevertheless, the mechanism(s) by which loss of PHEX function leads to the altered degradation and production of FGF-23 remains unknown. Thus, development of new therapeutic strategies for XLH has been limited and the disease remains incurable. Indeed, the failure of PHEX overexpression in *hyp*-mice to rescue the phenotype and of FGF-23 antibody treatment to completely resolve the bone mineralization abnormalities in mutant mice highlight the incomplete understanding of the pathophysiological mechanisms regulating FGF-23 degradation and production.[24–28]

Because FGF-23 is not a PHEX substrate in vivo,[29] the increased circulating levels of FGF-23 likely result from a downstream effect of the *PHEX/Phex* loss-of-function mutations. One potential mechanism by which this may occur is decreased activity of a prohormone convertase (PC), resulting in impaired cleavage at the RXXR motif. Indeed, transfection experiments have revealed that furin effectively cleaves FGF-23,[12,14,29,30] although uridine diphosphate-N-acetyl-alpha-D-galactosamine: polypeptide N-acetylgalactosaminyltransferase 3 (GALNT3)-mediated glycosylation near the cleavage site appears to modulate this effect.[31,32] Whether other PCs cleave this precursor has not been examined.

Although a downstream effect of the *PHEX/Phex* mutation may alter FGF-23 cleavage by limiting the activity of a PC, this effect must also enhance FGF-23 production, to provide complete explanation for the increased serum hormone levels. Previous in vitro studies have documented that dentin matrix acidic phosphoprotein 1 (DMP1), with three potential nuclear localization signals at the carboxy-terminus, localizes as a transcriptional factor to regulate gene expression.[33,34] Moreover, the recent observations that: (1) full-length DMP1 is an inactive precursor and proteolytic processing is an activation step essential to its biological functions; and (2) overexpression of the 57-kDa DMP1 C-terminal fragment in bone rescues the FGF-23 mediated hypophosphatemic rachitic phenotype of the *Dmp1* null mouse,[35,36] suggest that alteration of DMP1 degradation may influence FGF-23 production.[37,38] Thus, decreased PC activity due to the *PHEX/Phex* mutation may also inhibit DMP1 proteolysis, limiting the production of the C-terminal fragment and consequently enhancing *Fgf*--23 mRNA.

In this work we report the role that PCs play in the pathophysiology of XLH. We demonstrate that PC2 and its binding protein 7B2 are expressed in osteoblasts and that PC2 is a critical enzyme mediating FGF-23 degradation, as well as production, by promoting bone morphogenetic protein 1 (BMP1)-mediated cleavage of DMP1 and thereby altering *Fgf-23* mRNA transcription. In addition, we document that both transcription of the *Sgne1* (7B2) gene and active 7B2 protein levels are diminished in the *hyp*-mouse osteoblast, decreasing PC2 enzyme activity and leading to increased serum FGF-23 and the *HYP* phenotype. Most importantly, we establish that hexa-D-arginine treatment of *hyp*-mice corrects the abnormal *Sgne1* (7B2) transcription and 7B2 protein levels in osteoblasts and normalizes the biochemical phenotype, as well as completely healing the rickets/osteomalacia characteristic of XLH.

Subjects and Methods

Normal and *hyp*-mice

Normal C57BL/6J mice were mated with C57BL/6J heterozygous *hyp*-mice (Jackson Animal Laboratories, Bar Harbor, ME, USA) as described.[39] Hemizygotic male and heterozygotic female weanling *hyp*-mice, obtained from the resultant litters, were identified and selected for study, at 2 to 3 weeks of age by genotyping and/or serum phosphorus levels. Equal numbers of male and female normal littermates were chosen for investigation. All mice received a diet containing 0.6% calcium and phosphorus (Teklad Co., Madison, WI, USA) and deionized water *ad libitum* from the time of weaning until study. Care of mice met or exceeded the standards set forth by the National Institutes of Health in the Guidelines for the Care and Use of Laboratory Animals (NIH publication 86–23, revised 1985). The University of Wisconsin Animal Care and Use Committee approved all procedures. Experimental mice were euthanized by intraperitoneal (i.p.) injection of sodium pentobarbital.

Effects of Decanoyl-Arg-Val-Lys-Arg-Chloromethyl Ketone Administration in Normal Mice

Male and female C57BL/6J mice, aged 6 to 7 weeks, were randomly divided into a control and experimental group with 12 mice per group. At the inception of the study, 6 mice from the control and experimental group were separated for baseline measurements. We administered saline solution or decanoyl-Arg-Val-Lys-Arg-chloromethyl ketone (Dec) 50 μM in saline solution i.p. for 12 days to the remaining control and experimental mice. During the study the mice received the standard diet noted above. For measurements at baseline and termination of the study, mice were euthanized and blood was obtained for assay of serum Pi and FGF-23 levels.

Kidneys (1/mouse) were excised for measurement of 25-hydroxyvitamin D [25(OH)D]-1α-hydroxylase enzyme activity, and the remaining kidney and femurs were collected for RNA and protein extraction.

Effects of Hexa-D-Arginine Amide Administration in Normal and *hyp*-Mice

We assessed the effects of hexa-D-arginine amide (D6R) treatment in normal and *hyp*-mice. Male and female normal and *hyp*-mice, aged 3 weeks, were randomly divided into control and treatment groups of at least 8/group. Control and treated mice from each strain received a daily i.p. injection of saline or D6R in saline (1.5 μg/g/day; R&D Biosystems, Emeryville, CA, USA) for 5 weeks. We obtained blood from the retro-orbital plexus daily for measurement of serum Ca and Pi and at day 35 for measurement of FGF-23 levels. Throughout the treatment period, mice received the standard diet noted above and were monitored for changes in behavioral activity and food and water intake to confirm health. All mice received an i.p. injection of Calcein green dye (5 mg/kg; MP Biomedicals, Santa Ana, CA, USA) and Alzarin complexone dye (20 mg/kg; Acros Organics, Fair Lawn, NJ, USA) 8 and 5 days before study termination, respectively. After 5 weeks (3 days following administration of Alzarin) kidneys (1/mouse) were excised for measurement of 25(OH)D-1α-hydroxylase enzyme activity, and the alternate kidneys and femurs (1/mouse) were collected for RNA and protein extraction. The remaining femurs were collected for bone micro–computed tomography (μCT) analysis and bone histomorphometry.

Biochemical measurements

Serum Pi levels were measured using a Phosphorus Liqui-UV kit from Stanbio Laboratory (Boerne, TX, USA), as described.[22] Serum calcium levels were assayed using a calcium Liquicolor kit from Stanbio Laboratory following the manufacturer's protocol.[22]

Serum intact FGF-23 levels were measured using an FGF-23 ELISA kit obtained from Kainos Laboratories (Tokyo, Japan), with antigenic specificity designed to measure the intact molecule. The standard curve and duplicate measurements were obtained following the protocol of the manufacturer. Serum FGF-23 levels were also measured using an ELISA kit, purchased from Immunotops International (San Clemente, CA, USA), with antigenic specificity directed at the C-terminus of FGF-23. Following the manufacturer's protocol, this assay measures both intact FGF-23 and the C-terminal FGF-23 fragments.

Expression Vectors

Fgf-23 *expression vector*

Full-length mouse *Fgf-23* cDNA was subcloned into the mammalian expression vector pcDNA3.1 (Invitrogen, Carlsbad, CA, USA) with a myc-His tag created at the C-terminus. The full-length mouse *Fgf-23* cDNA was obtained by PCR (Platinum *Pfx* Taq; Invitrogen), using a forward primer designed with a KpnI recognition site and a Kozak translational initiation sequence (5′-GGT ACC GCC ACC ATG CTA GGG ACC TG CCT TA-3′), and reverse primer, designed with an XbaI recognition site (5′-TCT AGA GAC GAA CCT GGG AA-3′). The resulting 771-bp product was electrophoresed on a 2% agarose gel, isolated, and purified (Qiagen, Valencia, CA, USA). This blunt-ended product (FGFkzkxba) was subcloned into the pCR-Blunt II-TOPO plasmid (Invitrogen) and was used to transform TOP10 chemically competent *E. coli* (Invitrogen) (TOPO FGFkzkxba). Transformants were selected using ampicillin (Invitrogen) lysogeny broth (LB) plates and DNAs from resistant colonies sequenced using the M13 Reverse and T7 primers. The cDNA fragment was released using KpnI and XbaI (New England Biolabs, Ipswich, MA, USA), gel purified (Qiagen) and subsequently ligated into the pcDNA 3.1/*myc*-His A plasmid (Invitrogen) using the LigaFast Rapid DNA Ligation System (Promega, Madison, WI, USA). This plasmid, FGFkzkMyc, was purified and sequenced to confirm that the *Fgf-23* cDNA was inserted in-frame with the Myc epitope of the plasmid. A wild-type *Fgf-23* cDNA plasmid was also created in the pcDNA3.2/*myc*-His vector using a reverse primer, designed with an XhoI recognition site (5′-CTC GAG TTC CTC TAC GTG GGC TGA AC-3′) (FGFkzkWT). The PCR product extends through the stop codon of the *Fgf-23* gene, thereby stopping transcription of the plasmid before the *myc* epitope is reached. Initial transfection experiments were done using both FGFkxkMyc and FGFkzkWT and provided similar results, suggesting the *myc*-His tail of the construct does not interfere with the gene expression and function. Therefore, the transfection experiments were done using FGFkzkMyc (*Fgf-23* construct), allowing easy purification of the *myc*-His tag.

DMP1 *expression vectors*

The murine full-length *Dmp1* coding region was used previously to generate transgenic mice, under the control of a 3.6-kb type I collagen promoter.[40] In the current study, the construct was subcloned into the EcoRI site of the expression vector pcDNA3.1 (Invitrogen). The clone was then sequenced to assure proper insertion and correct orientation.

The DMP1 C-terminal 57-kDa construct and mutant DMP1 construct were obtained as described.[41] Briefly, based on the cleavage sites identified in rat DMP1, the DMP1 C-terminal 57-kDa construct expressing the 57-kDa fragment was subcloned into an expression vector, containing the 3.6-kb rat type I collagen promoter, plus a 1.6-kb intron 1 at EcoRV and SalI sites, giving rise to the Col1α1-57-kDa construct. The mutant *Dmp1* construct was obtained with the DMP1 cleavage site mutated at D197A to resist cleavage.[41]

Pcsk2 *and* Sgne1 *expression vectors*

Mouse full-length *Pcsk2* (PC2) and *Sgne1* (7B2) cDNA clones (MGC clone ID: 5707923 and 5361810, respectively) were purchased from Invitrogen. The plasmids were transformed into TOP10 chemically competent *E. coli* (Invitrogen) using selected LB media, following the manufacturer's protocol. The plasmids were collected and purified by a plasmid extraction method (Qiagen), and the size of the insert cDNA was verified by restriction enzyme (NotI and SalI) digestion, following the recommendations of Invitrogen. The clones were also sequenced to confirm their identity.

Cell culture and in vitro transfection

Immortalized mouse osteoblast (TMob) cells were obtained as described,[42] maintained in α modified essential medium (α-MEM), supplemented with 10% fetal bovine serum (FBS), penicillin (100 U/mL), and streptomycin (100 μg/mL), in a humidified atmosphere of 10% CO_2, 90% air at 37°C, and split every 3 to 5 days to maintain subconfluence. In preparation for an experiment, cells were plated in six-well plates and grown for 12 to 14 days in α-MEM containing 10% FBS, penicillin, and streptomycin, supplemented with 5 mM β-glycerophosphate and 25 μg/mL ascorbic acid, and the culture medium was changed every 3 days.

Transfection of TMob cells was performed using Lipofectamine 2000 following the manufacturer's suggested protocol (Invitrogen) after optimization of DNA and Lipofectamine ratios. For single transfection studies, cells were cultured in medium until 80% confluent (90% for *Sgne1* [7B2] RNAi transfection), and transfected with either a full-length *Dmp1*, *Dmp1* C-terminal construct, mutant *Dmp1* construct, or *Sgne1* RNAi (Invitrogen). Cells were collected for total RNA and protein extraction 48 hours after the transfection. For triple-transfection studies TMob cells were initially transfected with an *Fgf-23* construct and 4 hours later with either *Pcsk2* or *Sgne1* alone or *Pcsk2* plus *Sgne1* constructs. After overnight incubation, cells and medium were collected as described earlier in this paragraph.

Analytical Methodology

In vitro assay of murine renal 25(OH)D-1α-hydroxylase activity

We assayed the maximum velocity of renal 25(OH)D-1α-hydroxylase enzyme activity in kidney homogenates by previously described methods.[22,23] Data are expressed as femtomoles 1,25$(OH)_2$D per minute per milligram (wet wt) of kidney.

Real-time–rt PCR assay of mRNA

We performed real-time (RT)-rt PCR assays to quantitate mRNA in bone and kidney from normal and *hyp*-mice, as well as TMob cells. To isolate total RNA from bone, we euthanized the mice and disarticulated the femurs. The femurs were trimmed of fat and the marrow was removed, prior to freezing in liquid nitrogen for storage at −80°C. To prepare the bone for RNA isolation, samples were homogenized into fine powder in liquid nitrogen using a porcelain mortar and pestle. We extracted the total RNA from the resultant powder, using the TRIzol protocol (Life Sciences Technology, Carlsbad, CA, USA), as described.[22] We quantitated *Fgf-23*, *Pcsk2* (PC2), *Dmp1*, *Bmp1*, and *Sgne1* (7B2) mRNA from the samples following the protocol described[22] and using the following gene-specific primers:

(*Fgf-23*, GenBank accession #MC_000072) forward primer: 5′-CTG CTA GAG CCT ATC CGG AC-3′; reverse primer: 5′-AGT GAT GCT TCT GCG ACA A-3′;
(*Pcsk2* (PC2), GenBank accession #NM_008792) forward primer: 5′-CAC TCC CAA AGA AGG ATG GA-3′; reverse primer: 5′-TAA GAG GCA TTT TGG CTG CT-3′;
(*Dmp1*, GenBank accession #NM_016779) forward primer: 5′-ACT CAC TGT TCG TGG GTG GT-3′; reverse primer: 5′-TTG TGG GAA AAA GAC CTT GG-3′;
(*Bmp1*, GenBank accession #NM_009755) forward primer: 5′-CAC TCC ACA GCA GGA AGT GA-3′; reverse primer: 5′-CTC AGT GAA AGC TCC GGT TC-3′;
(*Sgne1* (7B2), GenBank accession #NM_009162) forward primer: 5′-PBS-CCC CAA CAT AGT GGC AGA GT-3′; reverse primer: 5′-AAC TGG AAT TCT CGG CTG AA-3′.

We prepared kidney total RNA using the TRIzol reagent.[23] Renal *Npt2a* and *Cyp27b1* (25(OH)D-1α-hydroxylase) mRNA were quantitated by RT PCR employing the primers and the protocols described.[23]

After washing the TMob cells once with 1× PBS, total RNA was extracted, using 1 mL TRIzol reagent per well, and following the manufacturer's protocol.

In all cases the isolated total RNA concentration was measured and the reverse transcription reaction was performed with 5 μg of total RNA, using an iScript First Strand cDNA Kit from Bio-Rad (Hercules, CA, USA). Subsequently, RT-rt PCR was performed, using iTaq SYBR Green Supermix (Bio-Rad), with the specific primers noted above on an ABI 7000 Applied Biosystems Thermocycler (Foster City, CA, USA). GAPDH expression was also determined with each RT-PCR reaction as an internal control for data analyses. Data were collected quantitatively and the CT number corrected by CT readings of the corresponding internal GAPDH controls. Data from a minimum of six determinations (mean ± SEM) are expressed in all experiments as fold changes (relative expression).

Western blot analysis

We performed Western blot analysis to quantify protein concentrations from the bone and kidneys of normal and *hyp*-mice, as well as TMob cells. Disarticulated femurs, trimmed of all fat and marrow free, were frozen in liquid nitrogen at −80°C prior to homogenization into a fine powder in liquid nitrogen using a porcelain mortar and pestle. Subsequently the powder was transferred into T-PER Tissue Protein Extraction Reagent with Halt protease inhibitor (Thermo Scientific, Rockford, IL, USA). After three 30-second sonications, samples were centrifuged and supernatants were stored at −80°C until use.

Kidneys from the various animal models were rinsed free of blood with ice-cold saline and protein extracts were prepared using a modified protocol as described.[23] Briefly, tissues were homogenized in sucrose buffer containing 20 mM HEPES, 1 mM EDTA, 255 mM sucrose, 0.4 mM phenylmethylsulfonyl fluoride, and 2 μg/mL leupeptin. The homogenate was subjected to sonication for 30 seconds and then centrifuged at 1500*g* for 15 minutes, and the pellet containing mitochondrial protein, including 25(OH)D-1α-hydroxylase, was resuspended in the same buffer, aliquotted, and stored at −80°C until use. The supernatant from the centrifugation, which contained the plasma membrane proteins, was also collected for the measurement of sodium-dependent phosphate transporter 2a (NPT2a) protein.

We prepared protein from TMob cells using the sucrose buffer described in the previous paragraph. In brief, cells in plate wells

were washed once with PBS (1×) buffer. Thereafter, the cells were scraped from the plate and the cell suspension was centrifuged at 1500*g* for 5 minutes, after which the cell pellets were resuspended in the sucrose buffer. The suspension was sonicated for 30 seconds and centrifuged at 1500*g* for 15 minutes. The resulting cell pellet was again resuspended in the sucrose buffer and stored at −80°C until use.

For preparation of Western blots, a 20-μg aliquot of the protein extracts was electrophoresed in 10% SDS-PAGE gel and transferred to a nitrocellulose membrane. The membrane was washed and probed with an appropriate dilution of specific anti-mouse 25(OH)D-1α-hydroxylase antibody (The Binding Site, Birmingham, UK), anti-human NPT2a antibody (Alpha Diagnostic, International, San Antonio, TX, USA), anti-rat FGF-23 antibody (R&D Systems, Minneapolis, MN, USA), anti-rat DMP1 antibody (from L. Bonewald, University of Missouri–Kansas City, Kansas City, MO, USA), anti-human BMP1 (from D Greenspan, University of Wisconsin–Madison, Madison, WI, USA), or anti-mouse PC2 and anti-mouse 7B2 (Protein Group, Chicago, IL, USA). Subsequently, the membrane was probed with appropriate corresponding secondary antibodies. To quantify the immunoblotting signal, 6 mL of chemiluminescence detection solution (ECL Plus; Amersham, Van Nuys, CA, USA) was added, and the signal was detected by a fluorescence scanner (Storm 860; Amersham). The density of bands was analyzed using ImageQuant 5.2 software (Molecular Dynamics, Sunnyvale, CA, USA). The antibodies were subsequently stripped off by incubation in reprobing solution (62.5 mM Tris-HCL, 2% SDS, and 100 mM 2-mercaptomethanol, pH 6.7) for 30 minutes at 50°C. The membrane was then blocked and probed with specific anti-cytochrome *c* (for 25(OH)D-1α-hydroxylase protein) or β-actin antibody (for the remaining proteins) to verify the loading equivalence among samples.

In situ hybridization of PC2 and 7B2 in bone

In situ hybridization was performed using a digoxigenin (DIG)-labeled *Pcsk2* (PC2) or *Sgne1* (7B2) cRNA probe, prepared from a murine *Pcsk2* or *Sgne1* cDNA fragment with an RNA Labeling Kit (Roche, Indianapolis, IN, USA). The specific cDNA fragment was obtained by PCR using bone total RNA as the template with the following primers:

(*Pcsk2*) forward primer 5′-CAC TCC CAA AGA AGG ATG GA -3′; and reverse primer 5′-CAA CCG TCT TCC CAT TGT CT-3′;
(*Sgne1*) forward primer 5′-GGT TAA AAA TGG CCT CAA GG-3′) and reverse primer 5′-AAC CCA TCC AAT GCT TAT GT-3′).

In situ hybridization was performed on paraffin sections of bone from normal and *hyp*-mice by previously described methods.[35] Briefly, the hybridization temperature was set at 55°C and the excess probe was washed off at a temperature of 70°C. DIG-labeled nucleic acids were detected using an enzyme-linked immunoassay with a specific conjugated anti-DIG-alkaline phosphatase antibody and colored substrates, NBT and BCZP, according to the protocol of the manufacturer (Roche, Indianapolis, IN, USA). Hybridization signals were photographed with a Nikon E800 microscope (Nikon, Tokyo, Japan) and a Magnafine camera (Optronics, Goleta, CA, USA).

Bone Structure and Histomorphology

High-resolution radiography (X-ray) and μCT of femur

Femurs were removed and, after the surrounding muscles were digested, washed in PBS buffer and X-rayed using a Faxitron radiographic inspection unit (Model 8050-020; Field Emission Corporation) with digital image capabilities. To determine the length of the femur, bones were radiographed and the OsteoMeasure system (version 4.1; Atlanta, GA, USA) was used to measure the length from femur head to lateral condyle. Bone samples were also scanned in a μCT imaging system (vivaCT40; Scanco Medical, Bassersdorf, Switzerland) and data were analyzed as described.[37]

Visualization of bone morphology by Goldner staining

Nondecalcified sagittal sections from femurs were stained using the Goldner-Masson trichrome stain, as reported.[35] Sections were photographed using a Nikon microscope at 10× with Bioquant OSTEO v 7.20 software (R&M Biometrics, Nashville, TN, USA). Unmineralized osteoid, staining red-brown, and mineralized bone, staining green, were measured using the Bioquant interactive image analysis system (R&M Biometrics), enabling unbiased sampling, averaging of areas, and determination of the osteoid and mineralized area per total area.

Assessment of bone mineralization dynamics

To assess bone formation and mineral apposition rates, mice were euthanized 3 days after injection of the second fluorescent dye, as noted above in the section entitled Effects of Hexa-D-Arginine Amide Administration in Normal and hyp-Mice. The femurs were removed and fixed in 2% paraformaldehyde and 2.5% glutaraldehyde at room temperature for 4 hours before serial dehydration, as described.[35] Sections of 50 μm were cut using a Leitz 1600 saw microtome. To estimate mineralization dynamics, unstained sections were viewed under epifluorescent illumination, using a Nikon PCM-2000 confocal microscope, coupled to an Eclipse E800 upright microscope, and interfaced with Osteomeasure histomorphometry software, version 4.1 (OsteoMetrics, Inc., Decatur, GA, USA).[35]

Statistical Analysis

Data are expressed throughout as the mean ± SEM. We evaluated the data statistically employing a Student's *t* test for two-group or treatment comparisons. For multiple group comparison, we used one-way ANOVA, and when a difference was established, the Holm-Sidak method was employed to determine which groups were significantly different. A *p* value of less than 0.05 was considered statistically significant.

Results

Effects of convertase inhibition in normal C57BL/6J mice

In initial studies, we investigated if a decrease in convertase activity, a potential downstream effect of the *PHEX/Phex* mutation, results in abnormalities of phosphorus, vitamin D, and FGF-23 homeostasis in normal mice, which are characteristic

of the *HYP* phenotype. Administration of the general convertase inhibitor, Dec, to C57Bl/6J mice for 12 days (50 μM/kg/d i.p.) significantly decreased the serum Pi level (7.20 ± 0.27 versus 5.41 ± 0.10 mg/dL; $p < 0.05$) (Supplementary Fig. S1A) to values approaching those seen in *hyp*-mice.[22] In contrast, the serum calcium concentration remained unchanged (9.10 ± 0.20 versus 8.93 ± 0.40 mg/dL). The decline in the serum Pi level was due to a commensurate decrease in renal *Npt2a* mRNA (1.06 ± 0.1 versus 0.69 ± 0.01 relative expression; $p < 0.05$) and NPT2a protein (0.98 ± 0.02 versus 0.58 ± 0.03 relative expression; $p < 0.01$) and the likely associated renal Pi wasting (Supplementary Fig. S1A).

Further study revealed that Dec-treated normal mice also exhibited aberrant regulation of renal 25(OH)D-1α-hydroxylase activity (Supplementary Fig. S1B). Thus, whereas the renal *Cyp27b1* (25(OH)D-1α-hydroxylase) mRNA (1.04 ± 0.04 versus 1.79 ± 0.05 relative expression; $p < 0.01$) was significantly increased in Dec-treated mice, consistent with hypophosphatemia, expression of the 25(OH)D-1α-hydroxylase protein (1.02 ± 0.03 versus 0.98 ± 0.06 relative expression) was unchanged compared to untreated animals. Accordingly, 25(OH)D-1α-hydroxylase activity (4.60 ± 0.40 versus 3.70 ± 0.20 fmol/min/mg) was unaltered. These changes reflect the unique translational abnormality in the regulation of vitamin D metabolism previously observed in *hyp*-mice.[23]

To establish if the biochemical and metabolic changes observed in the Dec-treated mice occurred through a similar mechanism to that operative in *hyp*-mice, we studied production and degradation of FGF-23 following treatment (Supplementary Fig. S1C). The serum FGF-23 concentration in treated mice was significantly elevated compared to controls (92.0 ± 8.80 versus 225 ± 14.60 pg/mL; $p < 0.01$). Moreover, Dec treatment resulted in a significant increase in bone *Fgf-23* mRNA ($1.00 \pm .27$ versus 2.3 ± 0.7 relative expression; $p < 0.01$) and FGF-23 protein levels (0.98 ± 0.03 versus 1.29 ± 0.11 relative expression; $p < 0.05$). Further in vitro studies confirmed and extended these observations (Supplementary Fig. S1D). Overnight incubation of Dec (25 μM) with TMob cells (mouse osteoblasts) not only enhanced *Fgf-23* mRNA (1.2 ± 0.2 versus 6.1 ± 1.5 relative expression; $p < 0.01$) and full-length FGF-23 protein (1.0 ± 0.2 versus 5.3 ± 0.6 relative expression; $p < 0.01$), but impaired FGF-23 degradation, as evidenced by Western blots documenting decreased C-terminal FGF-23 fragments in the medium (1.0 ± 0.18 versus 0.07 ± 0.001 relative expression; $p < 0.001$), despite the increased protein levels. Thus, the emergence of the *HYP* phenotype in Dec-treated mice was likely dependent on changes in FGF-23 production and degradation, characteristically observed in *hyp*-mice.[22,23]

Convertase Tissue Distribution

Because Dec inhibits the family of proprotein convertases, we examined the expression of the seven known convertases in TMob cells and in normal and *hyp*-mouse bone to potentially identify the specific enzyme responsible for the putative intracellular degradation and enhanced FGF-23 production in osteoblasts/bone. Furin, PC2, PC4, and PC7 are expressed at the mRNA level in TMob cells (Supplementary Fig. S2A) and in bone samples from normal and *hyp*-mice (Supplementary Fig. S2B). Additional investigation of murine tissues revealed that furin, PC4, and PC7 are widely expressed in a variety of organs, including brain, lung, heart, liver, spleen, kidney, and skeletal muscle, whereas PC2 is expressed only in the brain and in bone (Supplementary Fig. S2C). Because PC2 cleaves precursor proteins[43,44] and is uniquely colocalized with PHEX in osteoblasts/bone, this convertase was a candidate protein to regulate PHEX-dependent FGF-23 production and cleavage in bone.

Regulation of FGF-23 Cleavage and Production In Vitro

To establish the potential role of PC2 in regulating FGF-23 homeostasis, we initially examined the effects of 7B2 (a chaperone protein required for PC2 activity[45]), and/or PC2 on FGF-23 cleavage in cultured cells. For these studies we serially transfected TMob cells with *Fgf-23*, and 4 hours thereafter with *Sgne1* (7B2), *Pcsk2* (PC2), or *Sgne1* and *Pcsk2*. After incubation overnight, cells were collected for measurement of intact FGF-23, and culture medium for measurement of C-terminal fragments. Western blots revealed that neither 7B2 nor PC2 alone cleaved intact FGF-23 (Fig. 1*A*). However, transfection with both *Sgne1* and *Pcsk2* significantly increased the concentration of C-terminal fragments in the culture medium (Fig. 1*A*). Such increased cleavage likely occurred at the convertase consensus site between amino acids 179 and 180.[8–10] These data support the possibility that the 7B2•PC2 complex may play a role in bone FGF-23 metabolism.

Subsequently, to define a potential role for 7B2 and PC2 in the production of *Fgf-23* mRNA, we singularly transfected TMob cells with *Sgne1* (7B2) RNAi or a *Sgne1* (7B2)-encoding expression vector. Forty-eight hours after transfection with *Sgne1* RNAi, *Fgf-23* mRNA increased significantly (Fig. 1*B*). In accordance with the increased production of *Fgf-23* mRNA, the culture medium from transfected cells exhibited increased FGF-23 protein, but a decreased level of the FGF-23 C-terminal fragment, consistent with inhibited protein degradation (Fig. 1*C*). In contrast, transfection of TMob cells with a *Sgne1* (7B2) expression vector resulted in a significant decrease in *Fgf-23* mRNA (1.05 ± 0.0001 versus 0.59 ± 0.11 relative expression; $p < 0.01$) and a decrease in the level of intact FGF-23 (1.0 ± 0.2 versus 0.63 ± 0.1 relative expression; $p < 0.05$).

To explore whether the 7B2•PC2 regulation of *Fgf-23* mRNA production involves DMP1,[36–38] we assessed if DMP1 regulates FGF-23 production in osteoblasts. Initially, we transfected TMob cells with normal or mutated *Dmp1*-expression vectors. Overexpression of DMP1 reduced *Fgf-23* mRNA, while overexpression of proteinase-resistant mutant DMP-1 had no impact (Fig. 2*A*). Consistent with these observations, transfection of TMob cells with the C-terminal DMP1 fragment (57 kDa) resulted in significantly reduced *Fgf-23* mRNA production (Fig. 2*A*). These data suggest that DMP-1 cleavage and production of the C-terminal fragment may regulate *Fgf-23* mRNA production.

Subsequently, we examined whether *Sgne1* (7B2) and *Pcsk2* (PC2) expression regulates DMP1 cleavage in osteoblasts. Serial transfection of TMob cells with the *Dmp1* and *Sgne1* and *Pcsk2* expression vectors resulted in increased levels of N- and C-terminal DMP-1 proteolytic fragments, and in accord a decrease in intact DMP1 (Fig. 2*B*). In agreement with these findings,

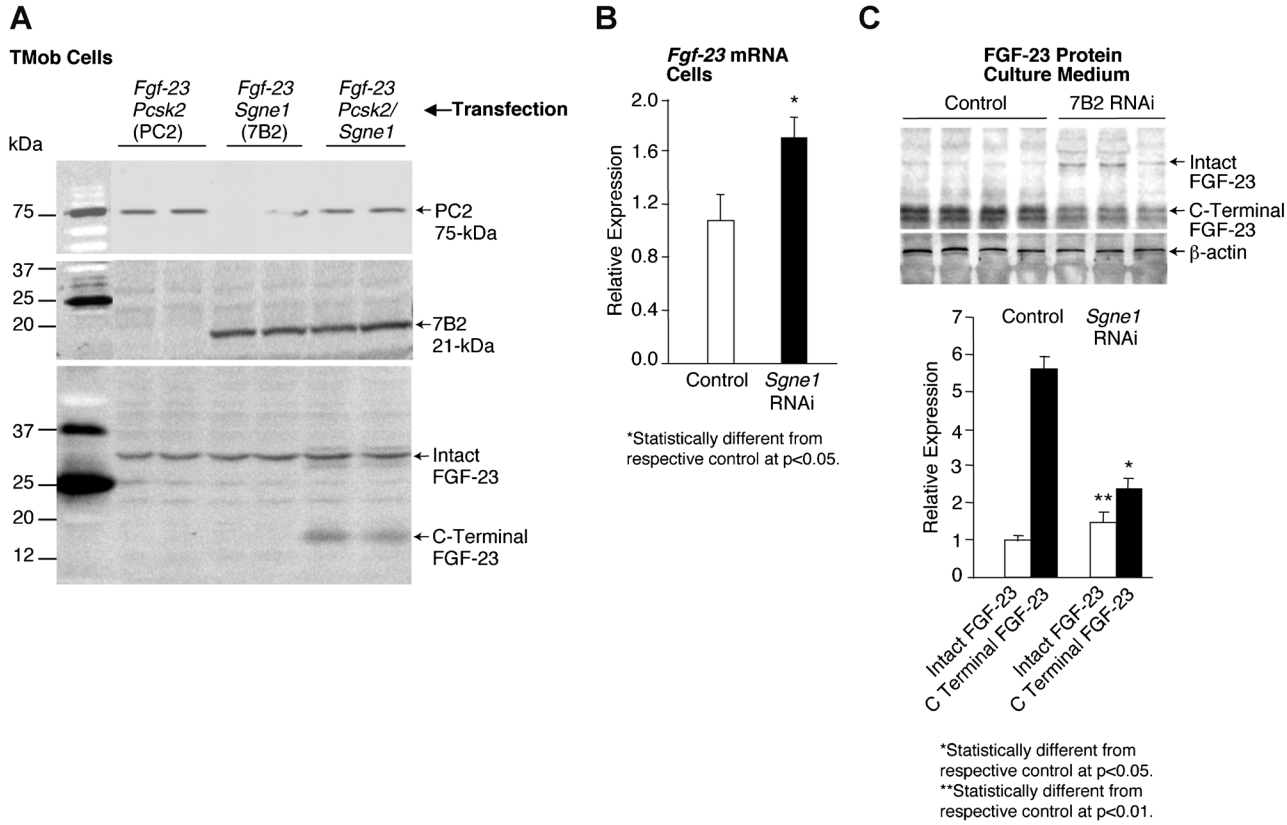

Fig. 1. Regulation of FGF-23 cleavage and production by 7B2•SPC2. (*A*) In TMob cells serially transfected with *Fgf-23*, and 4 hours thereafter with *Pcsk2* (PC2), *Sgne1* (7B2), or *Signe1* and *Pcsk2*, Western blots indicate that neither PC2 nor 7B2 alone cleaves intact FGF-23 to its C-terminal fragment. In contrast, the coincident transfection of PC2 and 7B2 cleaves the FGF-23, as evidenced by increased levels of C-terminal FGF-23 fragments in the cells. (*B*) Transfection of TMob cells with *Sgne1* (7B2) RNAi alone revealed that a significant increase in the *Fgf-23* mRNA occurs in the TMob cells, contributing to the presence of increased intact FGF-23. (*C*) Further analysis revealed that the diminished *Sgne1* mRNA and 7B2 protein resulted in a significant increase in the intact FGF-23 protein, but a significant decrease in the C-terminal FGF-23 in the culture medium, consistent with the anticipated diminished degradation of FGF-23 due to decreased 7B2•PC2 activity.

transfection of TMob cells with *Sgne1* RNAi, although having no effect on *Dmp1* mRNA, significantly increased the intact DMP1 due to a decrease in the levels of the DMP-1 N- and C-terminal cleavage products compared to that in controls (Fig. 2*C*).

Although these studies indicate that 7B2-dependent PC2 activity may regulate *Fgf-23* mRNA expression by altering DMP-1 cleavage, proteolytic processing of DMP-1 occurs at a site that is not a known substrate for PC2. Indeed, the only known enzyme that cleaves DMP-1, exclusively to the C-terminal 57-kDa carboxy-terminal and 37-kDa amino-terminal fragments, is BMP1, a tolloid-like proteinase that is activated by PC-mediated removal of an N-terminal prodomain.[46,47] Thus, we extended our studies to determine whether the 7B2-regulated PC2 activity cleaves the N-terminal prodomain of BMP1. Transfection of TMob cells with *Sgne1* RNAi had no effect on *pro-Bmp1* mRNA, but decreased the levels of active BMP1 and as a result significantly increased proBMP1 levels (Fig. 2*D*), consistent with 7B2•PC2-mediated cleavage of proBMP1 to active BMP1. Collectively, these findings support the possibility that PC2, in association with its binding protein 7B2, directly affects both degradation of the intact FGF-23 protein, and indirectly affects regulation of *Fgf-23* mRNA, by controlling proBMP1 cleavage to active BMP1 and the downstream proteolytic cleavage of the transcriptional regulator DMP-1.

Expression of 7B2 and PC2 in *hyp*-Mouse Bone

To confirm a role for 7B2 and PC2 in the regulation of FGF-23 in *hyp*-mice, we explored if decreased 7B2•PC2 activity was present in the bones from mutant mice, due to decreased expression of 7B2 and/or PC2. In situ hybridization studies documented a significant decrease in *Sgne1* (7B2) mRNA in the bones from *hyp*-mice and comparable levels of *Pcsk2* (PC2) mRNA in bones from normal and mutant mice (Fig. 3*A*). These results were confirmed by measurement of *Sgne1* and *Pcsk2* mRNA by RT PCR in normal and *hyp*-mouse bone samples (Fig. 3*B*). In accord, Western blots revealed decreased pro-7B2 and active 7B2 in *hyp*-mouse bone (Fig. 3*C*). Moreover, consistent with the requirement of 7B2 to generate active PC2, in part through proteolysis,[45,48] blots revealed that *hyp*-mouse bone exhibited a significantly increased proPC2 and decreased active PC2 content (Fig. 3*C*). Collectively, these data suggest that decreased *Sgne1* mRNA and protein in the bones of *hyp*-mice result in failure to normally cleave proPC2, and diminished 7B2•PC2 activity.

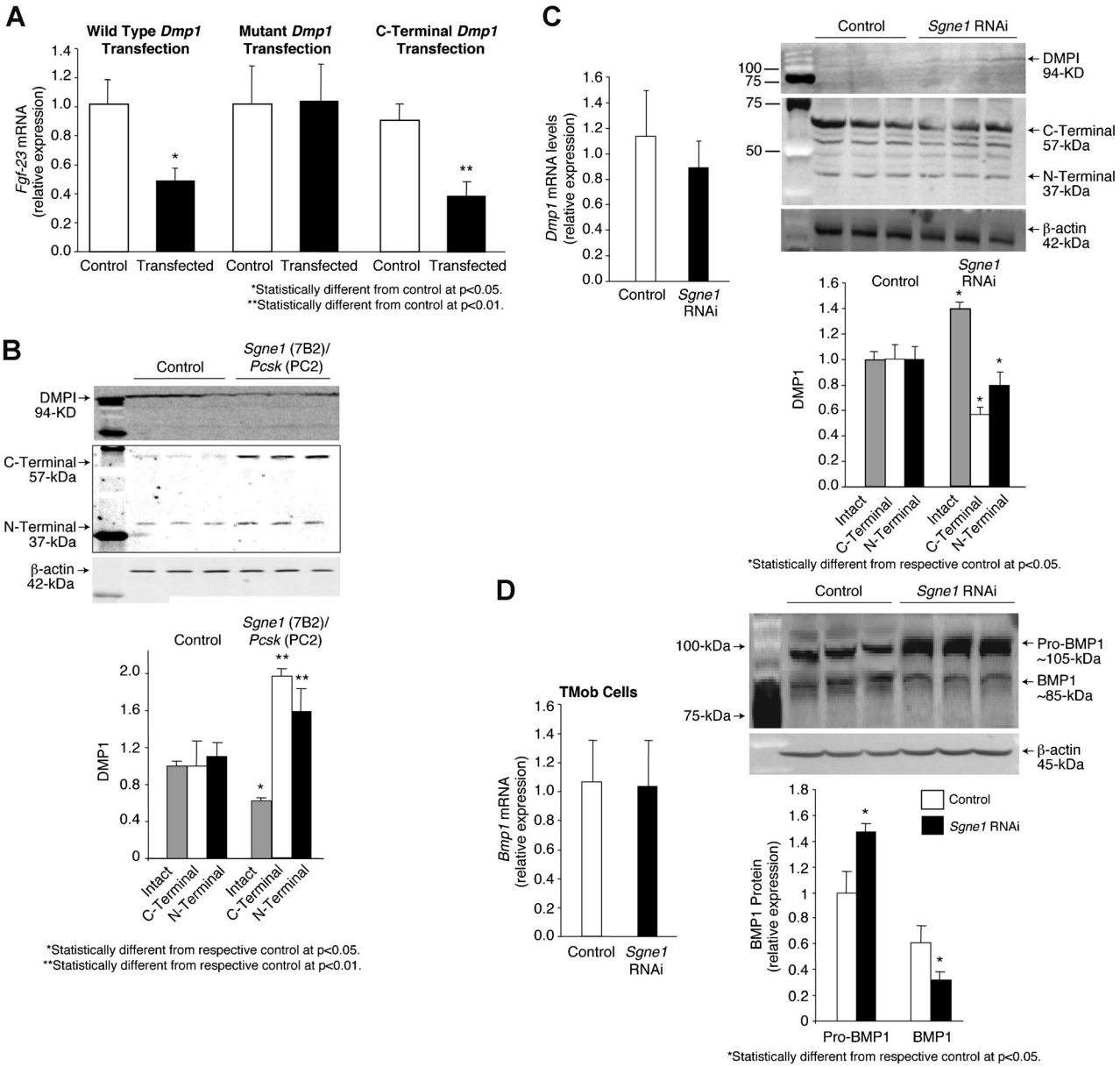

Fig. 2. DMP1 regulation of FGF-23 in osteoblasts. (*A*) Transfection of TMob cells with normal *Dmp1*, and resultant overexpression, reduced *Fgf-23* mRNA expression significantly. In contrast, transfection of TMob cells with proteinase resistant *Dmp1* had no effect on *Fgf-23* mRNA expression in the TMob cells, suggesting that DMP1 proteolysis is essential to regulate *Fgf-23* mRNA production. In accord, transfection of TMob cells with the C-terminal DMP1 fragment significantly decreased *Fgf-23* mRNA expression, supporting the role of DMP1 proteolysis in regulation of *Fgf-23* mRNA. (*B*) Serial transfection of TMob cells with *Dmp1* and *Pcsk2* (PC2) and *Sgne1* (7B2) resulted in Western blot evidence of a significant increase in C-terminal and N-terminal DMP1 fragments, and a consequent decrease in the intact DMP1, consistent with 7B2●PC2 mediation of DMP1 proteolysis as a possible factor in regulation of *Fgf-23* mRNA production. (*C*) Transfection of TMob cells with *Sgne1* RNAi had no effect on *Dmp1* mRNA production, but resulted in a significant decrease in the C-terminal and N-terminal DMP1 fragments, and a consequent increase in the intact DMP1, consistent with diminished proteolysis, further supporting a role for DMP1 cleavage in 7B2●PC2 regulation of *Fgf-23* mRNA production. (*D*) Transfection of TMob cells with *Sgne1* (7B2) RNAi had no effect on *Bmp1* mRNA, when compared to controls, but did result in a significant decrease in active BMP1 and a resultant increase in Pro-BMP1, changes consistent with 7B2●PC2 mediated activation of BMP1 serving as the mechanism that regulates DMP1 degradation.

The decreased 7B2●PC2 activity in *hyp*-mouse bone was accompanied by a profound increase in the serum FGF-23 concentration (Fig. 4*A*), resulting from increased *Fgf-23* mRNA in the *hyp*-mouse bone (Fig. 4*B*) and decreased degradation (Fig. 4*C*). Consistent with in vitro studies, the mechanism underlying the increased Fgf-23 mRNA was suggested by the presence of normal *Bmp1* mRNA in the bones of *hyp*-mice, but Western blot evidence of significantly increased proBMP1 and decreased active BMP1 levels (Fig. 4*D*), likely due to the diminished 7B2●PC2 activity. In accord, *Dmp1* mRNA was no different from normal in the *hyp*-mouse bone, but Western blots revealed increased levels of intact DMP-1, due to limited Bmp1-mediated degradation, as evidenced by decreased levels of N- and C-terminal DMP-1 cleavage products in the bones from mutant mice (Fig. 5*E*). These data are consistent with the hypothesis that decreased 7B2●PC2 activity in *hyp*-mouse bone

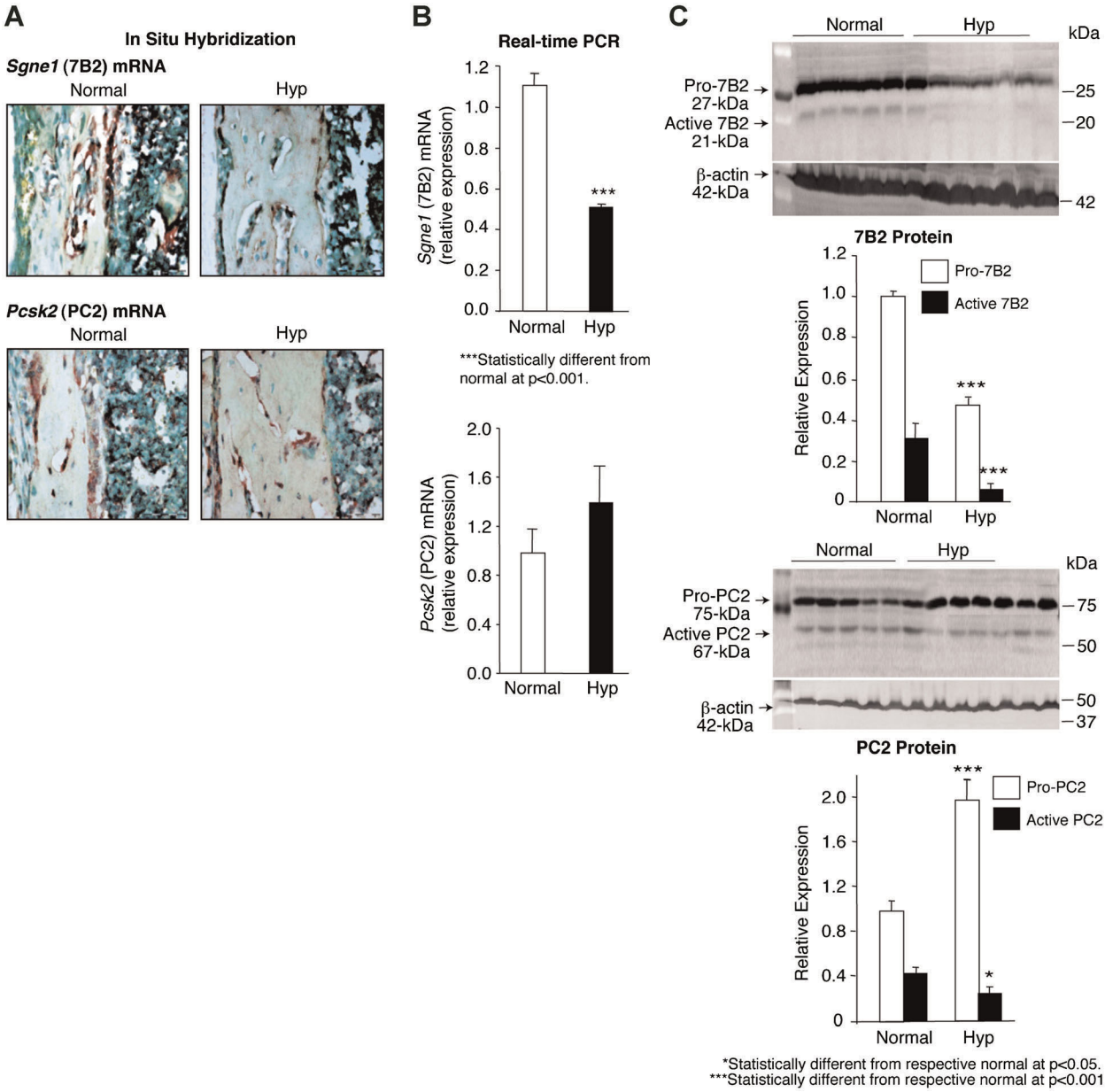

Fig. 3. Expression of 7B2 and PC2 in the bones from normal and *hyp*-mice. (*A*) In situ hybridization studies documented that the brown-staining *Sgne1* (7B2) mRNA was present in abundance in the bone sections from normal mice, but was clearly substantially decreased in the bone sections from *hyp*-mice; in contrast, no apparent difference in the *Pcsk2* (PC2) mRNA was detectable in bone sections from normal and *hyp*-mice. (*B*) Consistent with the observations made by in situ hybridization, real-time PCR measurements revealed significantly less *Sgne1* mRNA in *hyp*-mouse than in normal mouse bone samples, whereas no difference in *Pcsk2* mRNA was found. (*C*) In accord, assessment of 7B2 protein content in the bone samples, employing Western blots, documented significantly less pro-7B2 and active 7B2 protein in the *hyp*-mouse than in the normal bone samples. In the presence of diminished active 7B2 and consequent decreased PC2 proteolysis, the Western blots revealed significantly increased pro-PC2 content in the *hyp*-mouse bone and decreased mature PC2.

increases circulating levels of FGF-23 by limiting cleavage directly, and by increasing *Fgf-23* mRNA indirectly, via the BMP1-DMP1 pathway (Supplementary Fig. S2).

Effects of Normalizing 7B2 and Enhancing 7B2•PC2 Activity on the *HYP* Phenotype

In subsequent studies, we treated *hyp*-mice with hexa-D-arginine amide (D6R) to determine if therapeutic enhancement of bone 7B2 production and 7B2•PC2 activity normalized the *HYP* phenotype. D6R was chosen because: (1) polyarginines are the only known stimulant of PC2 activity;[49] (2) of the frequent coordinate regulation of 7B2 and PC2[50]; and (3) preliminary studies documented that overnight incubation of TMob cells with D6R (50 μM) significantly increased *Sgne1* (7B2) mRNA (1.0 ± 0.2 versus 2.8 ± 0.6 relative expression; $p < 0.01$).

Treatment of normal and *hyp*-mice for 5 weeks with either vehicle (saline) or D6R (1.5 μmol/g/day, i.p.) significantly increased the *Sgne1* (7B2) mRNA and 7B2 protein to levels no different than those in normal mice (Fig. 5*A*). These observations

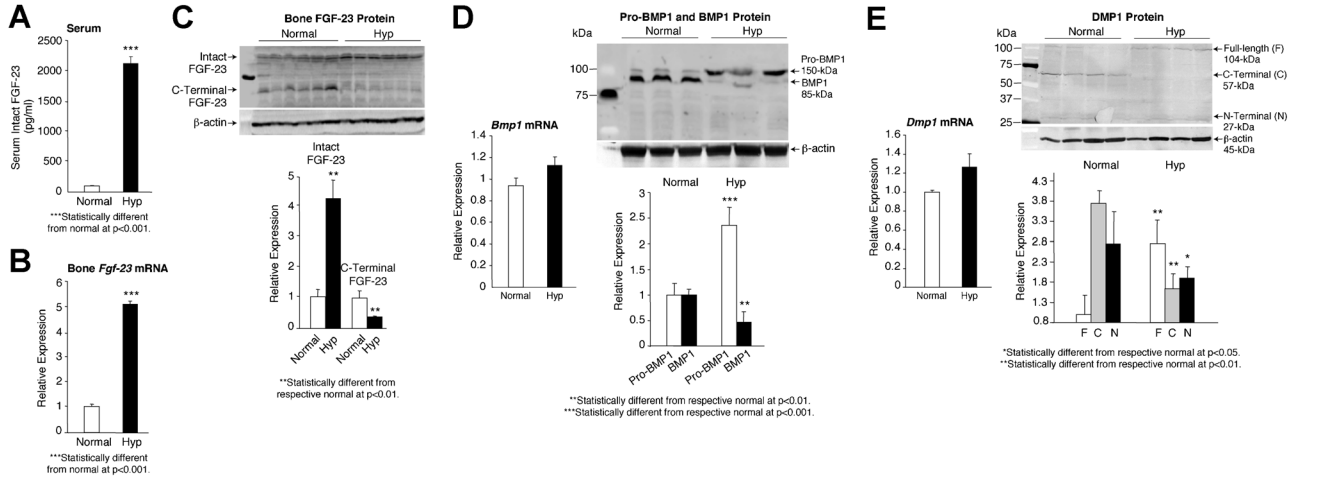

Fig. 4. Regulation of FGF-23 in normal and *hyp*-mice. (*A*) Serum FGF-23 levels, measured by an assay specific for the intact molecule, was profoundly elevated in the *hyp*-mice, when compared to normal mice. (*B*) Consistent with this observation, real-time PCR measurements documented that *Fgf-23* mRNA was likewise substantially elevated in the *hyp*-mouse bone samples. (*C*) Assessment of FGF-23 protein in the bone samples revealed a significant increase in intact FGF-23, but a significant decrease in the C-terminal FGF-23 fragments, evidence for impaired degradation. (*D*) Real-time PCR measurements of *Bmp1* mRNA in bone samples from normal and *hyp*-mice revealed no difference in expression. However, assessment of BMP1 protein in these samples by Western blots documented that the pro-BMP1 protein was significantly increased and the active BMP1 significantly decreased in the *hyp*-mouse bone samples, consistent with impaired 7B2●PC2 cleavage of the pro-BMP1, as observed in the in vitro studies. (*E*) Real-time PCR measurements of *Dmp1* mRNA in bone samples from normal and *hyp*-mice similarly revealed no difference in expression. However, consistent with decreased active BMP1 cleavage of DMP1, the bone samples from *hyp*-mice displayed a significant reduction in the N- and C-terminal DMP1 fragments and, as a result, significantly increased amounts of the full-length DMP1.

suggest that D6R treatment, by normalizing the 7B2 protein content, increased the 7B2●PC2 enzyme activity in *hyp*-mouse bone. Indeed, further studies revealed that the 7B2●PC2-dependent intermediate steps in FGF-23 production, including osteoblast production of active BMP1 (Fig. 5*B*) and proteolytic degradation of DMP1 to its 57-kDa C-terminal product (Fig. 5*C*) were normalized. Consequently, D6R treatment decreased *Fgf-23* mRNA expression to levels no different than those in normal mice (Fig. 5*D*).

Subsequent evaluation of bone from D6R-treated *hyp*-mice revealed restoration of normal bone length, as well as bone modeling and mineralization. As shown in Fig. 6*A*, saline-treated *hyp*-mice had shortened femurs, characteristic of the *HYP* phenotype. However, D6R treatment resulted in lengthening of the femurs from *hyp*-mice, while having no apparent effect on normal femurs. Indeed, measurement of femur length in normal and *hyp*-mice documented not only a significant shortening in the saline-treated mutants, but a significant increase in the D6R-treated *hyp*-mice to values approaching those in normal mice (Fig. 6*A*).

Further examination of the femurs by μCT revealed that saline-treated *hyp*-mice had poor mineralization of bone, associated with abnormal bone modeling. Whole-mount and sagittal bone sections from saline-treated *hyp*-mice displayed the classical features of rickets, including reduced length, increased width, porous bone, wider growth plates, and an enlarged diaphysis (Fig. 6*B*). Treatment with D6R restored bone modeling and calcification, reducing the width of the bones, decreasing porosity, and restoring normally sized growth plates and diaphyses. Similarly, μCT images of femur midshaft sections revealed increased porosity, an apparent reduced bone volume, and a commensurately enlarged cortical diameter. Again, D6R treatment showed restoration of normal bone architecture (Fig. 6*C*). The changes observed in μCT images of femur midshaft sections were confirmed by quantified bone volumetric data. Bone from the D6R-treated *hyp*-mice displayed a significant increase in bone volume, achieving values no different from those in normal mice (Fig. 6*C*).

These observations were supported by analysis of Goldner-stained bone sections obtained from saline- and D6R-treated mice (Fig. 6*D*). Compared to similarly treated normal mice, saline-treated *hyp*-mice had abundant brown-staining osteoid, distributed in widened seams over the bone surface and within pockets found in the mineralized trabecular bone. D6R treatment of *hyp* mice abolished the excess osteoid and quantitative histomorphology revealed that the osteoid in the D6R-treated *hyp*-mice significantly declined to levels no different than those in normal mice. Reciprocally, the mineralized area also normalized (Fig. 6*E*). Assessment of the bone mineral apposition rate confirmed the presence of normal mineralization (Fig. 6*F*). Whereas saline-treated normal mice displayed evidence of crisp double fluorescent bone labels, indicative of normal mineralization, fluorescent labeling in the long bones of *hyp*-mice was diffuse and smudged, indicative of abnormal mineralization. D6R treatment had no effect on the crisp double labels in normal mice, while remarkably altering mineralization dynamics in *hyp*-mice, inducing distinct double labels in the bone sections, consistent with normal mineralization. Quantitative histomorphology revealed that a profoundly decreased mineral apposition rate in saline-treated *hyp*-mice increased to normal levels upon treatment with D6R (Fig. 6*G*).

We further examined D6R-treated *hyp*-mice to determine if therapy also normalized the *HYP* biochemical abnormalities.

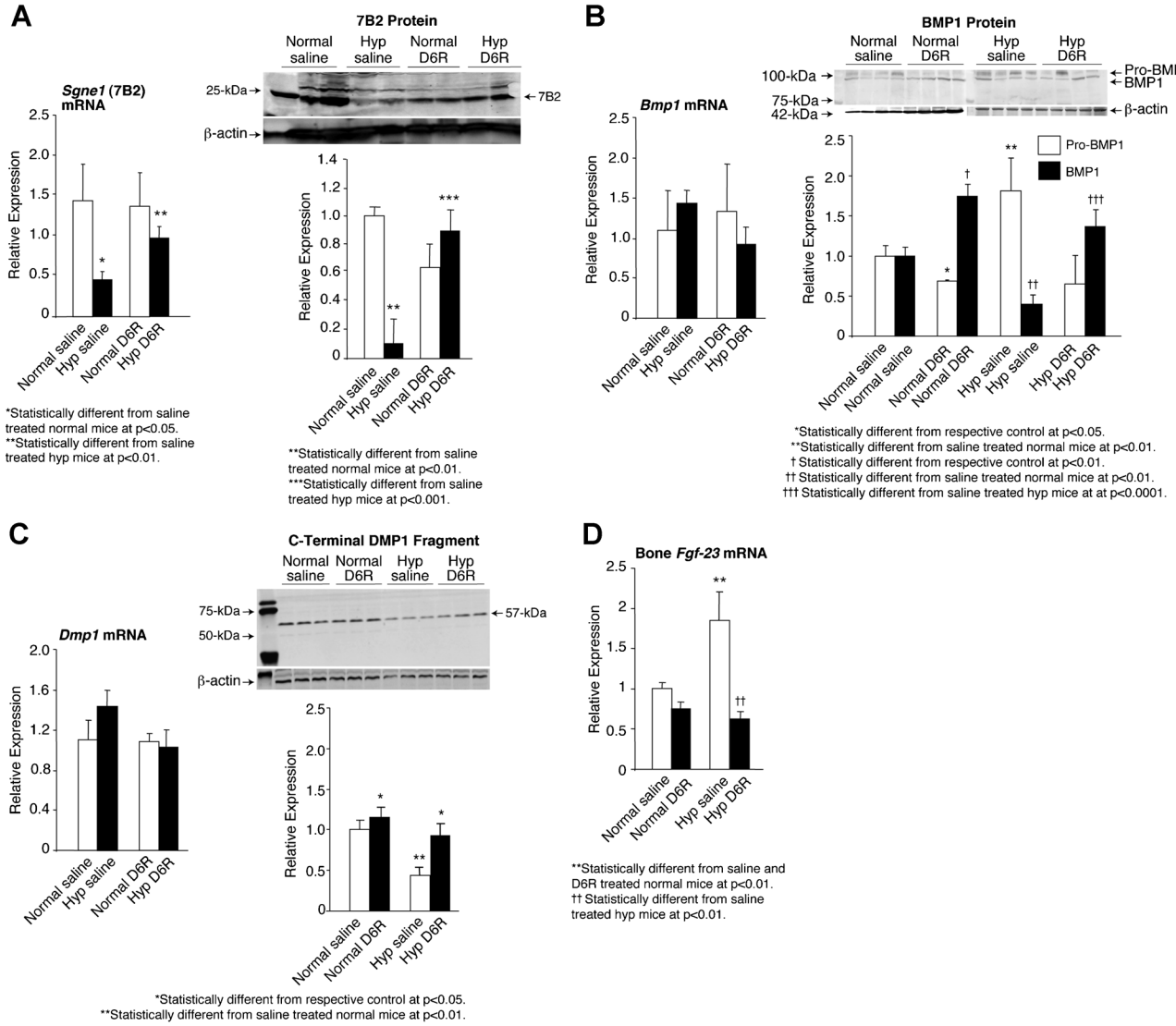

Fig. 5. Effects of D6R treatment on regulation of FGF-23 in normal and *hyp*-mice. (*A*) Real-time PCR measurements revealed a significant decrease in *Sgne1* (7B2) mRNA in the bone from saline-treated *hyp*-mice. With D6R treatment of the *hyp*-mice for 5 weeks, a significant twofold increase in *Sgne1* mRNA was realized, reaching levels no different than those in normal mice. Assessment of 7B2 protein by Western blots likewise documented a significant decrease in the saline-treated *hyp*-mice. In accord with the D6R-mediated enhancement of *Sgne1* mRNA, the active protein increased significantly, again reaching a level comparable to those in the normal mice. (*B*) Real-time PCR measurements revealed that D6R treatment had no effect on *Bmp1* mRNA in the bones of normal and *hyp*-mice. However, in response to treatment, the mutant mice normalized expression of the BMP1 active protein in bone samples, as evidenced on Western blots. Thus, although saline treated *hyp*-mice had significantly elevated pro-BMP1 and decreased active BMP1 in the bone samples, D6R treatment normalized the pro-BMP1 content and significantly increased the active BMP1 in *hyp*-mouse bone to levels no different than that in saline-treated mice. (*C*) Real-time PCR measurements revealed that D6R treatment had no effect on *Dmp1* mRNA in the bones of normal and *hyp*-mice. However, D6R-treated mutant mice significantly increased the C-terminal DMP1 fragments to levels within the normal range, as evidenced on Western blots, reflecting increased proteolysis of the intact DMP1. The intact DMP1 (94 kDa) is not shown on the Western blots, because no bands were evident, despite loading substantial amounts of protein, due to efficient proteolysis, consistent with previous observations.[37,71] (*D*) Real-time PCR measurements documented that *Fgf-23* mRNA was substantially elevated in the bone samples from saline-treated *hyp*-mouse bone samples, compared to that in saline-treated normal mice. However, D6R treatment of *hyp*-mice remarkably decreased the *Fgf-23* mRNA to values no different than those documented in the saline- and D6R-treated normal mice.

Administration of D6R to *hyp*-mice increased the serum Pi asymptotically from a baseline of 3.2 ± 0.2 mg/dL to a maximum of 6.6 ± 0.4 mg/dL ($p < 0.001$) (Fig. 7*A*). A significant increase in the serum Pi concentration was evident after only 3 days of treatment, and the serum Pi increased progressively to a peak at 21 days of treatment. Perhaps more importantly, whereas the serum Pi levels in the D6R-treated *hyp*-mice from days 0 to 18 were significantly less than those in the saline- and D6R-treated normal mice, values from 21 to 35 days of treatment were significantly greater than those at 18 days and no different than those in the normal mice (Fig. 7*A*). Normalization of the serum Pi occurred due to an increase of renal tubule *Npt2a* mRNA and NPT2a protein, to levels comparable to those in saline- or D6R-treated normal mice (Fig. 7*B*).

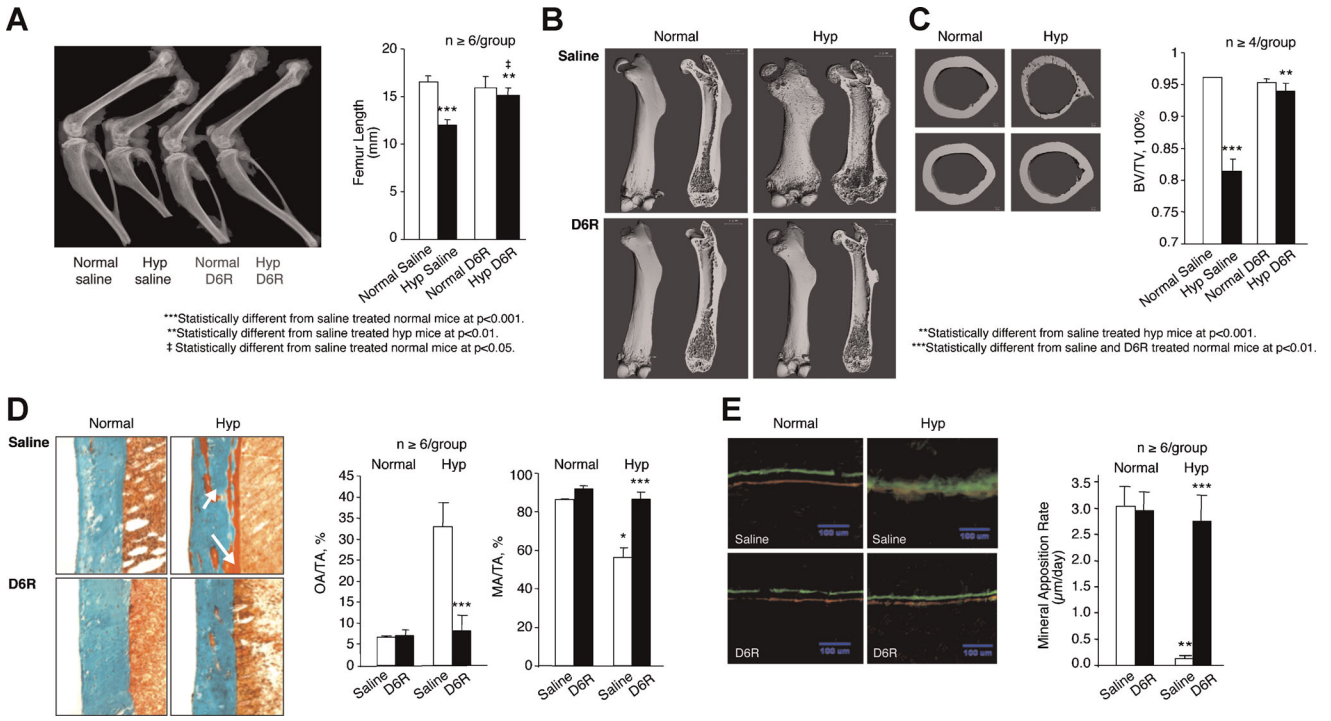

Fig. 6. Effects of D6R treatment on the *HYP* bone phenotype. (*A*) A representative radiograph of femurs in the saline and D6R-treated mice reveals that D6R treatment lengthens the characteristically shortened femur in *hyp*-mice to a length no different than that in normal mice, an observation confirmed by quantified data shown on the right. (*B*) Representative μCT images of the femurs from normal and *hyp*-mice treated with saline (upper panel) or D6R (lower panel) are shown with the whole-mount view on the left and sagittal sections on the right. The bone from saline-treated normal mice displays the classical rachitic features of rickets, porous bone, wide growth plates, and a large diaphysis. Treatment with D6R, however, restored normal bone modeling and calcification, resulting in normal bone architecture. (*C*) Representative μCT images of femur midshaft sections from saline (upper panel) and D6R-treated (lower panel) normal and *hyp*-mice. Bones from the saline-treated *hyp*-mice was porous and had an apparent reduced bone volume and enlarged cortical diameter, abnormalities normalized by D6R treatment, as confirmed by quantified data shown on the right. (*D*) Goldner-stained sections of cortical bone reveal at high magnification an increase in unmineralized osteoid (red-brown colored) in the saline-treated *hyp*-mouse bone, compared with that in saline- and D6R-treated normal mice. However, D6R-treatment of *hyp*-mice resulted in apparently normal histomorphology, as confirmed by quantitative assessment of osteoid area (OA/TA) and mineralized area (MA/TA), shown on the right. (*E*) Calcein green and Alizarin complexone dye double-labeled bone specimens, viewed under fluorescent light, show abnormal mineralization in the bone sections from saline-treated *hyp*-mice, as evidenced by smudged fluorescent labels, which are in marked contrast to the distinct dual labels evident in normal mice. However, D6R treatment of *hyp*-mice resulted in the presence of distinct dual fluorescent labels, set apart a similar distance as in normal mice. As shown on the right, these observations were confirmed by quantitative assessment of the mineral apposition rate, which was normal in the bone sections from D6R-treated *hyp*-mice.

Additionally, in response to D6R treatment, the increased renal *Cyp27b1* (25(OH)D-1α-hydroxylase) mRNA expression seen in hyp-mice decreased to values similar to those in saline- and D6R-treated normal mice (Fig. 7*C*). The unchanged expression of 25(OH)D-1α-hydroxylase protein and activity in D6R-treated *hyp*-mice (Fig. 7*C*) suggested that treatment had corrected the abnormal translational regulation of enzyme activity in the mutant mice.

However, as shown in Fig. 7*E*, although the serum FGF-23 concentration in D6R-treated *hyp*-mice decreased significantly, when measured by the intact and carboxy-terminal specific assays the level remained substantially increased. The elevated serum FGF-23 level persisted, despite normalization of bone *Fgf-23* mRNA (Fig. 5*D*), complete resolution of the *HYP* phenotype, and no end organ evidence of increased Fgf-23 bioactivity. Nevertheless, because the magnitude of the decrement was less, when examined using the carboxy-terminal specific assay, it is likely that the D6R treatment had increased hormone degradation, and treated *hyp*-mice had a relative increase in the circulating levels of the FGF-23 carboxy-terminal fragments.

Discussion

Despite apparent progress in understanding the pathophysiological basis for XLH, few advances have been made in defining an effective treatment for the disease. This failure is related to a unique block to treatments based on genetic complementation in this disorder. Classic complementation therapy has been precluded in this single-gene (*PHEX/Phex*) defect disease by the inability to rescue the phenotype by overexpression of PHEX[24–26] in *hyp*-mice and the failure to define a PHEX substrate.[21] However, discovery that a major PHEX-dependent abnormality in XLH is increased circulating FGF-23, which is strongly associated with the genesis of the *HYP* phenotype, appeared to offer a realistic alternative strategy for treatment via blockade of FGF-23 effects. Unfortunately, this approach has been severely limited

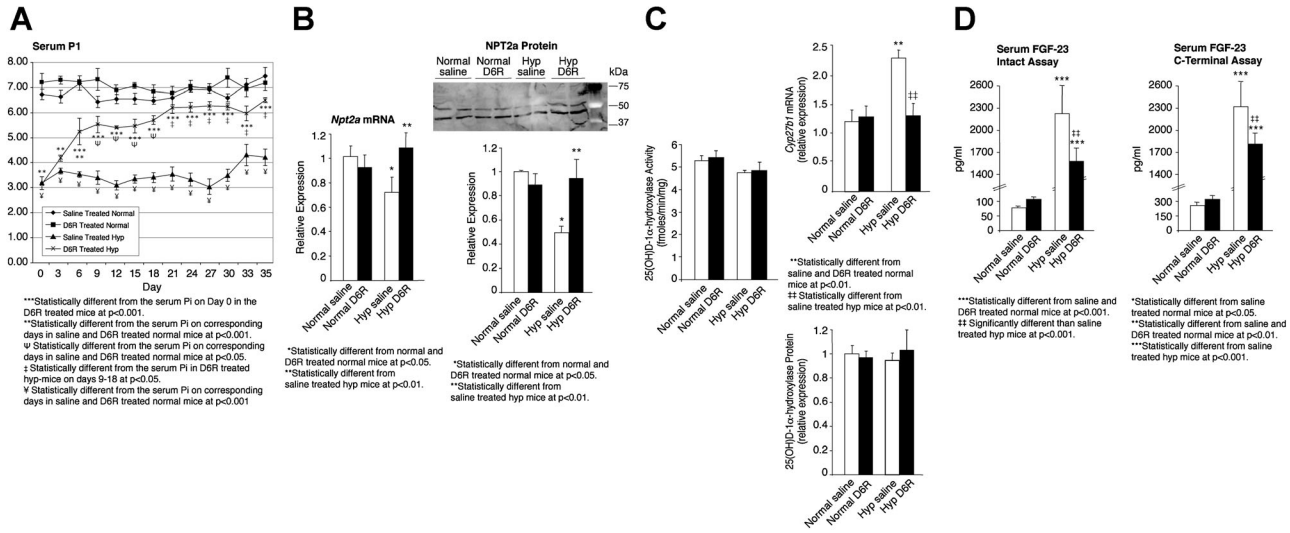

Fig. 7. Effects of D6R treatment on phosphate, vitamin D, and FGF-23 homeostasis in *hyp*-mice. (*A*) The 5-week D6R treatment course significantly increased the serum phosphorus concentration, compared to baseline, from day 3 through day 35. The increase in the serum phosphorus concentration in the D6R-treated *hyp*-mice progressed asymptotically, with values from days 3 to 18 significantly lower than those in the saline and D6R-treated normal mice. However, at the asymptotic maximum from days 21 to 35 of treatment, the serum phosphorus level was significantly greater than those from days 3 to 18, but more importantly no different than those in the saline- and D6R-treated normal mice. Throughout the treatment period the saline-treated *hyp*-mice maintained a serum phosphorus concentration significantly less than the D6R-treated *hyp*-mice and the saline- and D6R-treated normal mice. (*B*) The normalization of the serum phosphorus concentration in the D6R-treated *hyp*-mice was accompanied by a significant increase in the real-time measurements of renal *Npt2a* mRNA expression at 35 days, to values no different than those in saline- and D6R-treated normal mice. Similarly, the renal NPT2a protein content in the D6R-treated *hyp*-mice, assessed by Western blots, increased significantly to values no different than in saline- and D6R-treated normal mice. (*C*) Compared to saline-treated *hyp*-mice, the D6R-treated mutant mice displayed a significant decrease of the renal *Cyp27b1* (25(OH)D-1α-hydroxylase) mRNA expression to values no different than those in saline- and D6R-treated normal mice. The unchanging expression of the 25(OH)D-1α-hydroxylase protein and enzyme activity in the D6R-treated *hyp*-mice indicated that treatment had corrected the abnormal translational regulation of enzyme activity in the mutant mice. (*D*) Serum FGF-23 levels, measured by an assay specific for the intact molecule and a C-terminal specific assay, was profoundly elevated in the saline-treated *hyp*-mice. In concert with the normalization of *Fgf-23* mRNA (see Fig. 5*E*) and enhanced FGF-23 degradation, D6R treatment of *hyp*-mice significantly decreased the circulating FGF-23 levels, as measured by both assays. Comparing the data from the two assays, there is a 30% decrease, when using the measurement of intact FGF-23 and only a 24% decrease, when using the C-terminal assay, a difference consistent with an inordinate increase in the circulating C-terminal fragment likely due to a normalization of FGF-23 degradation.

by the incomplete response of the disease phenotype to antibody neutralization.[27,28]

Alternative approaches to modifying FGF-23 effects for a therapeutic purpose requires better understanding the mechanisms underlying the decreased degradation and increased production of this phosphatonin in health and in XLH. In the current studies, we used a variety of traditional biochemical and molecular biological techniques to explore the regulation of FGF-23 degradation and production both in vitro and in vivo. We initially demonstrated that general inhibition of proprotein convertase activity in normal mice increased circulating levels of FGF-23, decreased serum phosphorus, and induced posttranscriptional inhibition of 25(OH)D-1α-hydroxylase activity, changes that recapitulate the cardinal biochemical features of the *HYP* phenotype. Upon ascertaining that PC2 was a likely candidate convertase contributing to regulating FGF-23, we investigated whether this enzyme can alter FGF-23 degradation and production in vitro.

Proprotein convertases are responsible for the tissue-specific processing of multiple polypeptide precursors in a wide variety of tissues and cell lines.[38,44,51,52] However, PC2 differs from other proprotein convertases in its specific requirement for a chaperone protein, 7B2. Numerous studies have shown that PC2 maturation and enzyme activity are uniquely regulated by 7B2, and that PC2 expressed in the absence of 7B2 is incapable of autoactivation or substrate cleavage.[46,53–57] In accord with these observations, we showed that transfection of TMob cells with *Sgne1* (7B2) and *Pcsk2* (PC2) results in FGF-23 cleavage, whereas expression of *Sgne1* or *Pcsk2* alone has no effect. Moreover, FGF-23 degradation is blocked in TMob cells by *Sgne1* RNA-induced knockdown of *Sgne1* expression. These findings are consistent with the known presence of a convertase cleavage site in FGF-23 between amino acids 179 and 180 in the Arg-Arg-His-Thr-Arg motif, which in ADHR limits FGF-23 proteolysis and increases serum FGF-23.[8–10] Although many previous studies have shown that furin can mediate cleavage at this site[29,58,59] and PC2 is capable of cleaving either at the Arg-Arg site, or at single arginines in the presence of an upstream arginine,[60] our investigations indicate that PC2 may play a larger role than furin in this cleavage event in bone.

Subsequent investigations revealed that 7B2•PC2 activity regulates not only FGF-23 degradation, but FGF-23 production as well. Thus, transfection of TMob cells with a *Sgne1* (7B2) expression vector significantly decreased *Fgf-23* mRNA, whereas an increase in *Fgf-23* mRNA was detected upon *Sgne1* (7B2) RNAi inhibition of mRNA and protein expression. Further experiments

linked the effects of decreased 7B2•PC2 activity on FGF-23 production to reduced proteolysis of proBMP1, which resulted in limited cleavage of DMP1 to its 37-kDa N- and 57-kDa C-terminal fragments. The apparent impact of DMP1 on FGF-23 supports an important role for DMP1 proteolysis in the regulation of *Fgf-23* mRNA expression. However, although the unique effects of BMP1 on DMP1 proteolysis were known,[46] the apparent role of PC2 on proBMP1 cleavage was somewhat unexpected, because Golgi-localized furin represents the dominant convertase responsible for this cleavage event in the only cell type tested thus far, HT1080 cells.[46] However, the Arg-Ser-Arg-Arg site cleaved within proBMP1 is a PC2 recognition cleavage site,[60] providing justification for further work to establish the contribution of PC2 to proBMP1 cleavage in bone cells and tissue.

It is important to note that BMP1 is not the only enzyme that cleaves DMP1. Recent studies[50] have documented that matrix metalloproteinase-2 (MMP2), a membrane-bound enzyme, also cleaves the intact DMP1. However, the cleavage products include a 42-kDa carboxy-terminal fragment, which appears to have biological effects in dental pulp. The absence of the DMP1 42-kDa carboxy-terminal fragment in the normal and *hyp*-mouse bone, or the TMob cells, indicates that the 7B2-PC2 mediated cleavage of DMP1 is dependent on generation of active BMP1.

Although these data clearly establish that decreased 7B2•PC2 activity is associated with reduced FGF-23 degradation and increased hormone production in vitro, the role that such altered enzyme function might play in XLH remained uncertain. Therefore, we examined whether defective expression of either 7B2 or PC2 occurred in *hyp*-mice. Bone obtained from the mutant mice exhibited significantly decreased expression of both *Sgne1* (7B2) mRNA and 7B2 protein. These decreased levels of 7B2 limit cleavage not only of FGF-23, but of proPC2 as well, as evidenced by the presence of an increased ratio of proPC2 to active PC2. These observations are consistent with previous reports in the *Sgne1* null mouse[45] and in cell culture,[48,55] and support the concept that reduction in 7B2 levels results in decreased bone PC2 activity in XLH.

The possibility that a primary defect in *hyp*-mice is reduced 7B2 was confirmed by further studies that revealed expected downstream effects of decreased 7B2•PC2 activity. As previously found,[22,23] *hyp*-mice exhibit significantly increased levels of serum FGF-23, as a result of both decreased FGF-23 degradation and increased FGF-23 production. Consistent with our in vitro studies, increased FGF-23 production in *hyp*-mouse bone was associated with decreased BMP1-mediated degradation of DMP1 and decreased genesis of the C-terminal DMP1 fragment. Although the increase in *Fgf-23* mRNA may not result directly from the decreased concentrations of the DMP1 carboxy-terminal fragment, our in vitro studies, and the recent reports that establish transgenic overexpression of the C-terminal DMP1 fragment is essential to rescue the *Dmp1* null phenotype and normalize serum FGF-23,[36–38] support DMP1 proteolysis-mediated regulation of FGF-23 production in the *hyp*-mouse. In summary, these results establish that diminished 7B2 production in bone represents a critical step in the pathogenesis of the *HYP* phenotype (Supplementary Fig. S3), although the mechanism(s) by which the *Phex* mutation causes downregulation of 7B2 expression in *hyp*-mice remains unknown.

Although the well-known functional link between 7B2 and PC2 implies that their expression is coordinately regulated, the data obtained in the *hyp*-mouse model support the idea of discordant regulation. Indeed, such discordant regulation has been previously reported. Thus, while stimulation of P19 neuronal cells via a protein kinase C-mediated pathway coordinately increases expression of both 7B2 and PC2, protein kinase A-mediated stimulation increases expression of PC2 alone.[60] Moreover, a growing body of evidence suggests 7B2 expression frequently controls PC2 activity in hormonal peptide production.[61] The molecular details of the control of 7B2 expression are only now beginning to emerge, with recent studies pointing to promoter polymorphisms which clearly control expression[57,62]; ie, a 5′ regulatory region in *Sgne1* (7B2) mRNA, which acts to repress expression[62] and epigenetic control by differential methylation of the *Sgne1* gene.[63–65] The relative contributions of these various regulatory mechanisms to the control of 7B2 expression in bone is not yet known.

Although our in vivo observations support the possibility that 7B2-dependent, PC2-mediated alterations in FGF-23 degradation and production are operative in the *hyp*-mouse osteoblast, the singular role of this abnormality in the genesis of the *HYP* phenotype was still unclear. To explore this issue further, we sought to pharmacologically normalize PC2 activity in order to increase FGF-23 degradation and decrease production. The effects observed in D6R-treated *hyp*-mice were indeed remarkable. As anticipated, treatment resulted in a significant increase in the bone *Sgne1* (7B2) mRNA and 7B2 protein and no doubt concordant enhancement of 7B2•PC2 enzyme, which resulted in apparent normalization of the *HYP* phenotype. Indeed, during the 5-week period of treatment, serum phosphorus levels increased progressively to values maintained from days 21 to 35 that were no different than those of normal mice. These changes were clearly secondary to a significant increase in the renal *Npt2a* mRNA and NPT2a protein. Likewise, administration of D6R corrected the abnormal translational regulation of renal 25-hydroxyvitamin D-1α-hydroxylase activity, characteristic of the *hyp*-mouse.

Further, D6R treatment not only normalized the biochemical abnormalities, but had profound effects on bone architecture, remodeling, and mineralization. Thus, bone length was returned to normal in the *hyp*-mice, as was bone modeling and mineralization. These changes resulted in long bones with normal width and size of the growth plates and diaphyses. Moreover, restoration of mineralization dynamics included establishing a normal mineral apposition rate and eliminating all evidence of excess unmineralized osteoid. Complete resolution of the rickets and osteomalacia in response to D6R treatment is in marked contrast to the effects of alternative therapeutic regimens. Previous treatment strategies for XLH in affected humans and mice have included vitamin D and phosphorus,[66] calcitriol and phosphorus,[67,68] antibody neutralization of Fgf-23,[28] and PHEX overexpression,[24–26] all of which invariably remarkably improve the biochemical phenotype, but uniformly fail to heal the bone disease, particularly the

osteomalacia. Thus, treatment with D6R influences bone mineralization in an unprecedented fashion.

The effects noted in the preceding paragraphs were those anticipated with the D6R-mediated increase in bone *Sgne1* mRNA and protein, and consequent enhanced 7B2•PC2 enzyme activity. Although the molecular mechanism by which D6R increases *Sgne1* message levels in bone cells remains unknown, the expected result of such enhanced activity is restoration of normal FGF-23 production and degradation, and accordingly reduction of the stimulus for the abnormal biochemistries and bone morphology and histology present in *hyp*-mice. Indeed, in response to D6R treatment we observed decreased transcription of *Fgf-23* mRNA, along with the predicted enhanced BMP1 activation and elevated proteolytic degradation of DMP1. However, the serum FGF-23 level in the D6R-treated *hyp*-mice remained elevated when measured using the intact and carboxy-terminal immunoassays. Nevertheless, comparison of the measurements by these techniques revealed a greater decrement when assessed using the intact immunoassay, suggesting that degradation of the intact FGF-23 was enhanced and perhaps normalized.

The explanation for this incongruous elevation of the serum FGF-23 concentration is not immediately apparent. Measurement of serum FGF-23 at multiple dilutions in D6R-treated *hyp*-mice produced results that diluted parallel to the standard curve, eliminating co-measurement of an unrelated factor. It is also unlikely that the bioactivity of the circulating FGF-23 is decreased by a limited interaction of the hormone with its receptor, FGF1R, due to either a decrease in the renal klotho protein, a key component of the binary complex that creates FGF1R,[69] or competitive inhibition of the intact FGF-23 binding to its receptor by the C-terminal FGF-23, consistent with recently reported findings.[70] It is possible that structural differences in the circulating FGF-23 in treated *hyp*-mice may influence measurement of the intact molecule, consistent with the extraosseous clearance of intact FGF-23, about which little is known. No data are available that indicate such degradation of circulating FGF-23 generates the classic N- and C-terminal fragments. With the absence of any evidence of increased bioactivity at the kidney or bone, it seems plausible that extraosseous degradation of remarkably elevated serum levels of intact FGF-23 may generate abundant amounts of a bioinactive FGF-23 fragment, which includes the antigenic epitope(s) recognized by the antibodies used in the ELISA measurement. Since the antigenic epitopes are at the N-terminal and C-terminal cleavage sites, the bioinactive fragment may result from cleavage of the intact FGF-23 at site(s) distal to the normal N- and C-terminal cleavage site, rendering the molecule bioinactive but preserving the antigenic epitopes. Additional studies, outside the scope of the present investigation, will be necessary to establish with certainty if the elevated serum FGF-23 level, in association with normal bioactivity at kidney and bone, represents interference of hormone binding to its receptor, circulation of a bioinactive fragment of FGF-23, detected by the ELISA assay, or another event.

Regardless, our studies indicate that the loss-of-function *Phex* mutation in *hyp*-mice results in decreased osseous 7B2 production, a protein essential for manifestation of PC2 activity. The loss of 7B2 results in diminished PC2 activity and significantly limits cleavage of FGF-23 and proBMP1 and, indirectly, of DMP1. The physiological consequences that ultimately result from the 7B2 defect are increased levels of circulating FGF-23 and consequent renal phosphate wasting, abnormal transcriptional regulation of renal 25-hydroxyvitamin D-1α-hydroxylase activity, and rickets/osteomalacia. Most importantly, we found that the polyarginine D6R apparently restores the activity of PC2, most likely by increasing 7B2 production. D6R thus normalizes the *HYP* phenotype, correcting phosphate and vitamin D homeostasis, as well as bone modeling and mineralization. Whereas much work remains to establish the cellular and molecular mechanisms for PHEX-7B2 interactions, the findings presented here provide novel insight into the biosynthetic mechanisms of FGF-23 synthesis, and, most importantly, create a biochemical basis for a fully curative drug treatment regimen for XLH.

Disclosures

Drs. Drezner and Yuan have filed a use patent for Hexa-D-Arginine, US Patent Application #13/272809, Drezner et al (patent pending). The authors have no other conflicts of interest.

Acknowledgments

This work was funded by NIH grants (R01-AR27032, R01-SK65830, and 1UL1RR025011 to MKD; R01-DE018486 to JQF; AR54753 to RDB; and DK049703 to IL) and a Veterans Administration grant to RD Blank (Merit Award). The work reported in this article was conducted in the VAMC Geriatrics Research, Education, and Clinical Center, Madison, WI, USA.

Authors' roles: Study design: MKD, BY, IL, and RDB. Study conduct: BY, SB and YL. Data collection: BY, SB, and YL. Data analysis: MKD, BY, IL, JQF, and RDB. Drafting of manuscript: MKD and BY. Revising of manuscript: MKD, BY, IL, JQF, and RDB. Obtained funding: MKD, JQF, RDB, and IL.

References

1. Rasmussen H, Tenenhouse HS. Mendelian hypophosphatemias. In: Scriver CR, Beaudet AL, Sly WS, Valle D, editors. The metabolic and molecular basis of inherited diseases. New York: Mc-Graw Hill Book Co; 1995. p. 3717–45.
2. [no authors listed]. A gene (PEX) with homologies to endopeptidases is mutated in patients with X-linked hypophosphatemic rickets. The HYP Consortium. Nat Genet. 1995;11:130–6.
3. Sabbagh Y, Tenenehouse HS. PHEXdb: PHEX Locus Database Search Engine Site [Internet]. Debelle Data Group; 1999 [cited 2012 Aug 19]. Available from http://www.phexdb.mcgill.ca/.
4. Holm IA, Huang X, Kunkel LM. Mutational analysis of the PEX gene in patients with X-linked hypophosphatemic rickets. Am J Hum Genet. 1997;60(4):790–7.
5. Du L, Desbarats M, Viel J, Glorieux FH, Cawthorn C, Ecarot B. cDNA cloning of the murine Pex gene implicated in X-linked hypophosphatemia and evidence for expression in bone. Genomics. 1996; 36(1):22–8.
6. Rowe PS, Oudet CL, Francis F, Sinding C, Pannetier S, Econs MJ, Strom TM, Meitinger T, Garabedian M, David A, Macher MA, Questiaux E, Popowska E, Pronicka E, Read AP, Mokrzycki A, Glorieux FH, Drezner MK, Hanauer A, Lehrach H, Goulding JN, O'Riordan JL. Distribution of

mutations in the PEX gene in families with X-linked hypophosphataemic rickets (HYP). Hum Mol Genet. 1997;6:539–49.

7. Beck L, Soumounou Y, Martel J, Krishnamurthy G, Gauthier C, Goodyer CG. Pex/PEX tissue distribution and evidence for a deletion in the 3′ region of the Pex gene in X-linked hypophosphatemic mice. J Clin Invest. 1997;99(6):1200–9.
8. The ADHR Consortium. Autosomal dominant hypophosphataemic rickets is associated with mutations in FGF-23. Nat Genet. 2000;26:345–8.
9. Bai XY, Miao D, Goltzman D, Karaplis AC. The autosomal dominant hypophosphatemic rickets R176Q mutation in fibroblast growth factor 23 resists proteolytic cleavage and enhances in vivo biological potency. J Biol Chem. 2003;278:9843–9.
10. White KE, Carn G, Lorenz-Depiereux B, Benet-Pages A, Strom TM, Econs MJ. Autosomal-dominant hypophosphatemic rickets (ADHR) mutations stabilize FGF-23. Kidney Int. 2001;60:2079–86.
11. Araya K, Fukumoto S, Backenroth R, Takeuchi Y, Nakayama K, Ito N, Yoshii N, Yamazaki Y, Yamashita T, Silver J, Igarashi T, Fujita T. A novel mutation in fibroblast growth factor 23 gene as a cause of tumoral calcinosis. J Clin Endocrinol Metab. 2005;90(1):5523–7.
12. Benet-Pages A, Orlik P, Strom TM, Lorenz-Depiereux B. An FGF23 missense mutation causes familial tumoral calcinosis with hyperphosphatemia. Hum Mol Genet. 2005;14(3):385–90.
13. Chefetz I, Heller R, Galli-Tsinopoulou A, Richard G, Wollnik B, Indelman M, Koerber F, Topaz O, Bergman R, Sprecher E, Schoenau E. A novel homozygous missense mutation in FGF23 causes familial tumoral calcinosis associated with disseminated visceral calcification. Hum Genet. 2005;118(2):261–6.
14. Larsson T, Yu X, Davis SI, Draman MS, Mooney SD, Cullen MJ, White KE. A novel recessive mutation in fibroblast growth factor-23 causes familial tumoral calcinosis. J Clin Endocrinol Metab. 2005;90(4): 2424–7.
15. Larsson T, Davis SI, Garringer HJ, Mooney SD, Draman MS, Cullen MJ, White KE. Fibroblast growth factor-23 mutants causing familial tumoral calcinosis are differentially processed. Endocrinology. 2005;146(9):3883–91.
16. Garringer HJ, Malekpour M, Esteghamat F, Mortazavi SM, Davis SI, Farrow EG, Yu X, Arking DE, Dietz HC, White KE. Molecular genetics and biochemical analyses of FGF23 mutations in familial tumoral calcinosis. Am J Physiol Endocrinol Metab. 2008;295(4):E929–37.
17. Larsson T, Marshll R, Schipani E, Ohlsson C, Ljunggren O, Tenenhouse HS, Juppner H, Jonsson KB. Transgenic mice expressing fibroblast growth factor 23 under the control of the α1(I) collagen promoter exhibit growth retardation, osteomalacia, and disturbed phosphate homeostasis. Endocrinology. 2004;145(7):3087–94.
18. Shimada T, Urakawa I, Yamazaki Y, Hasegawa H, Hino R, Yoneya T, Takeuchi Y, Fujita T, Fukumoto S, Yamashita, FGF-23 transgenic mice demonstrate hypophosphatemic rickets with reduced expression of sodium phosphate cotransporter type IIa. Biochem Biophys Res Commun. 2004;314:409–14.
19. Jonsson KB, Zahradnik R, Larsson T, White KE, Sugimoto T, Imanishi Y. Fibrolast growth factor 23 in oncogenic osteomalacia and X-linked hypophosphatemia. N Engl J Med. 2003;348:1656–63.
20. Yamazaki Y, Okazaki R, Shibata M, Hasegawa Y, Satoh K, Tajima T. Increased circulator level of biologically active full-length FGF-23 in patients with hypophosphatemic rickets/osteomalacia. J Clin Endocrinol Metab. 2002 Nov; 87(11):4957–60.
21. Liu S, Zhou J, Tang W, Jiang X, Rowe DW, Quarles LD. Pathogenic role of Fgf23 in *Hyp* mice. Am J Physiol Endocrinol Metab. 2006; 291(1):E38–49.
22. Yuan B, Takaiwa M, Clemens TL, Feng JQ, Kumar R, Rowe PS, Xie Y, Drezner MK. Aberrant Phex function in osteoblast and osteocytes alone underlies murine X-linked hypophosphatemia. J Clin Invest. 2008;118(2):722–34.
23. Yuan B, Xing Y, Horst RL, Drezner MK. Evidence for abnormal translational regulation of renal 25-hydroxyvitamin D-1-α-hydroxylase activity in the *Hyp*-mouse. Endocrinology. 2004;145(8):3804–12.
24. Liu S, Guo R, Tu Q, Quarles LD. Overexpression of Phex in osteoblasts fails to rescue the Hyp mouse phenotype. J Bio Chem. 2002; 277(1):3686–97.
25. Erben RG, Mayer D, Weber K, Jonsson K, Juppner H, Lanske B. Overexpression of human PHEX under the human β-actin promoter does not fully rescue the Hyp mouse phenotype. J Bone Miner Res. 2005;20(7):1149–60.
26. Bai X, Miao D, Panda D, Grady S, McKee MD, Goltzman D, Karaplis AC. Partial rescue of the Hyp phenotype by osteoblast-targeted PHEX (phosphate-regulating gene with homologies to endopeptidases on the X chromosome) expression. Mol Endocrinol. 2002;16:2913–25.
27. Yamazaki Y, Tamada T, Kasai N, Urakawa I, Aono Y, Hasegawa H, Fujita T, Kuroki R, Yamashita T, Fukumoto S, Shimada T. Anti-FGF23 neutralizing antibodies show the physiological role and structural features of FGF23. J Bone Miner Res. 2008;23:1509–18.
28. Aono Y, Yamazaki Y, Yasutake J, Kawata T, Hasegawa H, Urakawa I, Fujita T, Wada M, Yamashita T, Fukumoto S, Shimada T. Therapeutic effects of anti-FGF23 antibodies in hypophosphatemic rickets/osteomalacia. J Bone Miner Res. 2009;24:1879–88.
29. Liu S, Guo R, Simpson LG, Xiao ZS, Burnham CE, Quarles LD. Regulation of fibroblastic growth factor 23 expression but not degradation by PHEX. J Biol Chem. 2003;278:37419–26.
30. Bai X, Miao D, Li J, Goltzman D, Karaplis AC. Transgenic mice overexpressing human fibroblast growth factor 23 (R176Q) delineate a putative role for parathyroid hormone in renal phosphate wasting disorders. Endocrinology. 2004;145(11):5269–79.
31. Ichitawa S, Sorenson AH, Austin AM, Mackenzie DS, Fritz TA, Moh A, Hui SL, Econs MJ. Ablation of the Galnt3 gene leads to low-circulating intact fibroblast growth factor 23 (Fgf23) concentrations and hyperphosphatemia despite increased Fgf23 expression. Endocrinology. 2009;150(6):2543–50.
32. Kato K, Jeanneau C, Tarp MA, Benet-Pagès A, Lorenz-Depiereux B, Bennett EP, Mandel U, Strom TM, Clausen H. Polypeptide GalNAc-transferase T3 and familial tumoral calcinosis. Secretion of fibroblast growth factor 23 requires O-glycosylation. J Biol Chem. 2006;281(27): 18370–7.
33. He G, Dahl T, Veis A, George A. Dentin matrix protein 1 initiates hydroxyapatite formation in vitro. Connect Tissue Res. 2003; 44 (Suppl 1):240–5.
34. Narayanan K, Ramachandran A, Hao J, He G, Park KW, Cho M, George A. Dual functional roles of dentin matrix protein 1. J Biol Chem. 2003;278(19):17500–8.
35. Feng JQ, Ward LM, Liu S, Lu Y, Xie Y, Yuan B, Yu X, Rauch F, Davis SI, Zhang S, Rios H, Drezner MK, Quarles LD, Bonewald LF, White KE. Loss of DMP1 causes rickets and osteomalacia and identifies a role for osteocytes in mineral metabolism. Nat Genet. 2006;38(11):1310–5.
36. Lorenz-Depiereux B, Bastepe M, Benet-Pagès A, Amyere M, Wagenstaller J, Müller-Barth U, Badenhoop K, Kaiser SM, Rittmaster RS, Shlossberg AH, Olivares JL, Loris C, Ramos FJ, Glorieux F, Vikkula M, Jüppner H, Strom TM. DMP1 mutations in autosomal recessive hypophosphatemia implicate a bone matrix protein in the regulation of phosphate homeostasis. Nat Genet. 2006;38: 1248–50.
37. Lu Y, Yuan B, Qin C, Cao Z, Xie Y, Dallas SL, McKee MD, Drezner MK, Bonewald LF, Feng JQ. The biological function of DMP-1 in osteocyte maturation is mediated by its 57-kDa C-terminal fragment. J Bone Miner Res. 2011;26(2):331–40.
38. Sun Y, Prasad M, Gao T, Wang X, Zhu Q, D'Souza R, Feng JQ, Qin C. Failure to process dentin matrix protein 1 (DMP1) into fragments leads to its loss of function in osteogenesis. J Biol Chem. 2010;285:31713–22.

39. Lobaugh B, Drezner MK. Abnormal regulation of renal 25-hydroxyvitamin D-1 alpha-hydroxylase activity in the X-linked hypophosphatemic mouse. J Clin Invest. 1983;71(2):400–3.

40. Lu Y, Ye L, Yu S, Zhang S, Xie Y, McKee MD, Li YC, Kong J, Eick JD, Dallas SL, Feng JQ. Rescue of odontogenesis in Dmp1-deficient mice by targeted re-expression of DMP1 reveals roles for DMP1 in early odontogenesis and dentin apposition in vivo. Dev Biol. 2007; 303(1):191–201.

41. Lu Y, Qin C, Xie Y, Bonewald LF, Feng JQ. Studies of the DMP1 57-kDa functional domain both in vivo and in vitro. Cells Tissues Organs. 2009;189(1–4):175–85.

42. Xiao ZS, Creshaw M, Guo R, Nesbitt T, Drezner MK, Quarles LD. Intrinsic mineralization defect in Hyp mouse osteoblasts. Am J Physiol. 1998;275(4 Pt 1):E700–8.

43. Steiner DF. On the discovery of precursor processing. Methods Mol Biol. 2011;768:3–11.

44. Seidah NG. The proprotein convertases, 20 years later. Methods Mol Biol. 2011;768:23–57.

45. Zhu X, Lindberg I. 7B2 facilitates the maturation of proPC2 in neuroendocrine cells and is required for the expression of enzymatic activity. J Cell Biol. 1995;129(6):1641–50.

46. Leighton M, Kadler KE. Paired basic/furin-like proprotein convertase cleavage of pro-BMP1 in the trans-Golgi network. J Biol Chem. 2003;278:18478–84.

47. Steiglitz BM, Ayala M, Narayanan K, George A, Greenspan DS. Bone morphogenetic protein-1/tolloid-like proteinases process dentin matrix protein-1. J Biol Chem. 2004;279:980–6.

48. Westphal CH, Muller L, Zhou A, Zhu X, Bonner-Weir S, Schambelan M, Steiner DF, Lindberg I, Leder P. The neuroendocrine protein 7B2 is required for peptide hormone processing in vivo and provides a novel mechanism for pituitary Cushing's disease. Cell. 1999; 96(5):689–700.

49. Cameron A, Appel J, Houghten RA, Lindberg I. Polyarginines are potent furin inhibitors. J Biol Chem. 2000;275(47):36741–9.

50. Petit-Turcotte C, Paquin J. Coordinate regulation of neuroendocrine convertase PC2 and peptide 7B2 in P19 neurons. Peptides. 2000; 21(3):365–72.

51. Jansen E, Ayoubi TA, Meulemans SM, Van de Ven WJ. Neuroendocrine-specific expression of the human prohormone convertase 1 gene. Hormonal regulation of transcription through distinct cAMP response elements. J Biol Chem. 1995;270(25):15391–7.

52. Ohagi S, Sakaguchi H, Sanke T, Tatsuta H, Hanabusa T, Nanjo K. Human prohormone convertase 3 gene: exon-intron organization and molecular scanning for mutations in Japanese subjects with NIDDM. Diabetes. 1996;45(7):897–01.

53. Muller L, Cameron A, Fortenberry Y, Apletalina EV, Lindberg I. Processing and sorting of the prohormone convertase 2 propeptide. J Biol Chem. 2000;275(50):39213–22.

54. Braks JA, Martens GJ. 7B2 is a neuroendocrine chaperone that transiently interacts with prohormone convertase PC2 in the secretory pathway. Cell. 1994;78(2):263–73.

55. Seidel B, Dong W, Savaria D, Zheng M, Pintar JE, Day R. Neuroendocrine protein 7B2 is essential for proteolytic conversion and activation of proprotein convertase 2 in vivo. DNA Cell Biol. 1998; 17(12):1017–29.

56. Benjannet S, Savaria D, Chretien M, Seidah NG. 7B2 is a specific intracellular binding protein of the prohormone convertase PC2. J Neurochem. 1995;64(5):2303–11.

57. Farber CR, Chitwood J, Lee SN, Verdugo RA, Islas-Trejo A, Rincon G, Lindberg I, Medrano JF. Overexpression of Scg5 increases enzymatic activity of PCSK2 and is inversely correlated with body weight in congenic mice. BMC Genet. 2008;9:34–45.

58. Shimada T, Mizutani S, Muto T, Yoneya T, Hino R, Takeda S, Takeuchi Y, Fujita T, Fukomoto S, Yamashita T. Cloning and characterization of FGF23 as a causative factor of tumor-induced osteomalacia. Proc Natl Acad Sci U S A. 2001;98:6500–5.

59. Benet-Pages A, Lorenz-Depiereux B, Zischka H, White KE, Econs MJ, Strom TM. FGF23 is processed by proprotein convertases but not by PHEX. Bone. 2004;35:455–62.

60. Cameron A, Apletalina E, Lindberg I. The enzymology of prohormone convertases PC1 and PC2. In: Dalbey RE, editor. The enzymes. San Diego, CA, USA: Academic Press; p. 33–43. 2001.

61. Chaussain C, Eapen AS, Huet E, Floris C, Ravindran S, Hao J, Menashi S, George A. MMP2-cleavage of DMP1 generates a bioactive peptide promoting differentiation of dental pulp stem/progenitor cell. Eur Cell Mater. 2009;18:84–95.

62. Helwig M, Lee SN, Hwang JR, Ozawa A, Medrano JF, Lindberg I. Dynamic modulation of PC2-mediated precursor processing by 7B2: preferential effect on glucagon synthesis. J Biol Chem. 2011;266(4): 42504–13.

63. Schmidt G, Sirois F, Anini Y, Kauri LM, Gyamera-Acheampong C, Fleck E, Scott FW, Chretien M, Mbikay M. Differences of pancreatic expression of 7B2 between C57BL/6J and C3H/HeJ mice and genetic polymorphisms at its locus (Sgne1). Diabetes. 2006;55(2): 452–9.

64. Tadros H, Schmidt G, Sirois F, Mbikay M. Regulation of 7B2 mRNA translation: dissecting the role of its 5′-untranslated region. Methods Mol Biol. 2011;768:217–30.

65. Waha A, Koch A, Hartmann W, Milde U, Felsberg J, Hubner A, Mikeska T, Goodyer CG, Sorensen N, Lindberg I, Wiestler OD, Pietsch T, Waha A. SGNE1/7B2 is epigenetically altered and transcriptionally downregulated in human medulloblastomas. Oncogene. 2007; 26(38):5662–8.

66. Waha A, Felsberg J, Hartmann W, Hammes J, von dem Knesebeck A, Endl E, Pietsch T, Waha A. Frequent epigenetic inactivation of the chaperone SGNE1/7B2 in human gliomas. Int J Cancer. 2012;131(3): 612–22.

67. Lyles KW, Harrelson JM, Drezner MK. The efficacy of vitamin D2 and oral phosphorus therapy in X-linked hypophosphatemic rickets and osteomalacia. J Clin Endocrinol Metab. 1982;54:307–15.

68. Drezner MK, Lyles KW, Haussler MR, Harrelson JM. Evaluation of a role for 1,25-dihydroxyvitamin D_3 in the pathogenesis and treatment of X-linked hypophosphatemic rickets and osteomalacia. J Clin Invest. 1980;66:1020–32.

69. Nakatani T, Ohnishi M, Razzaque MS. Inactivation of klotho function induces hyperphosphatemia even in presence of high serum fibroblast growth factor 23 levels in a genetically engineered hypophosphatemic (Hyp) mouse model. FASEB J. 2009;23:3702–11.

70. Goetz R, Nakada Y, Hu MC, Kurosu H, Wang L, Nakatani T, Shi M, Eliseenkova AV, Razzaque MS, Moe OW, Kuro-o M, Mohammadi M. Isolated C-terminal tail of FGF23 alleviates hypophosphatemia by inhibiting FGF23-FGFR-Klotho complex formation. Proc Natl Acad Sci U S A. 2010;107:407–12.

71. Qin C, Brunn JC, Cook RG, Orkiszewski RS, Malone JP, Veis A, Butler WT. Evidence for the proteolytic processing of entin matrix protein 1. Identification and characterization of processed fragments and cleavage sites. J Biol Chem. 2003;278:34700–8.